Numerical Solver Module for the Gross-Pitaevskii Equation

Biruk Chafamo

Advisor: Professor Nathan Lundblad

Department of Physics and Astronomy
Bates College
Lewiston, ME 04240

April 18, 2022

Acknowledgments

I would like to thank my advisor professor Nathan Lundblad for his support and encouragement throughout this thesis. I want to especially thank my parents who pray for me each night. I would also like to thank my brothers to whom I owe my love for learning. Above all, I want to dedicate this thesis to Sosi for being by my side unconditionally.

Abstract

In this thesis, we discuss the theoretical background and implementation details of a software package in python that models the dynamics of Bose-Einstein condensates. In particular, the solution to the non-linear Gross-Pitaevskii equation for the condensate is solved using two separate algorithms. The first algorithm is the Split-Step Fourier method and the second is the Fourth-Order Runge-Kutta Interaction Picture method. The utility of the first algorithm comes from approximating an expression with two non-commuting operators as well as using the Fourier transformation to simplify the expensive matrix exponentiation of the non-diagonal kinetic operator in the Gross-Pitaevskii equation. The second algorithm applies a canonical transformation that decomposes the Gross-Pitaevskii equation into a system of ordinary differential equations that can be efficiently solved with the Fourth-Order Runge-Kutta method. These algorithms are applied in two separate ways. The first application is to solve the ground state solution of the Bose-Einstein condensate wave function using imaginary time evolution. The second application is to evolve the ground state solution across time after some external modification to the environment of the condensate. Lastly, this thesis presents a demonstration of the associated Python module by using it to simulate the dynamics of a Bose-Einstein condensate in different conditions.

Contents

1 Introduction **1**
- 1.1 Bose-Einstein Condensates: Overview . . . 1
- 1.2 Motivation and Outline . . . 1

2 Background **3**
- 2.1 Bose-Einstein Condensates . . . 3
  - 2.1.1 Preparation . . . 3
  - 2.1.2 Pauli-Exclusion Principle . . . 4
- 2.2 Gross-Pitaevskii Equation . . . 4
  - 2.2.1 Quantum Mechanics: Review . . . 5
  - 2.2.2 GPE Derivation . . . 7

3 Numerical Approach **9**
- 3.1 Setup . . . 9
  - 3.1.1 Dimensionless GPE . . . 9
  - 3.1.2 Computational Grid . . . 10
- 3.2 Algorithms . . . 11
  - 3.2.1 Split-Step Fourier Method . . . 11
  - 3.2.2 Interaction Picture Fourth-order Runge-Kutta . . . 13
  - 3.2.3 Adaptive Time-Step . . . 17

4 Ground State Solution **18**
- 4.1 Guessing Initial Wave Function . . . 18
- 4.2 Imaginary Time Evolution . . . 18

5 Simulations **21**
- 5.1 Finding the Ground State . . . 21
  - 5.1.1 Examples in 1-D . . . 21
  - 5.1.2 Example in 2-D . . . 24
- 5.2 Time Evolution . . . 27
  - 5.2.1 Example in 1-D . . . 27
  - 5.2.2 Examples in 2-D . . . 27

5.3 Interference 33
5.3.1 Example in 2-D 33
5.4 Performance Comparison 33

6 Conclusion **37**
6.1 Summary 37
6.2 Outlook 38

A Code Demonstration **39**
A.1 1-D Implementation 39
A.2 2-D Implementation 39

List of Figures

5.1 Guessed Wave Function in 1-D 22
5.2 Guessed Vs. Ground Wave Function in 1-D 23
5.3 Ground States Comparison in 1-D 24
5.4 Guessed Wave Function in 2-D 25
5.5 Guessed Vs Ground Wave Function in 2-D 26
5.6 Time Evolution in Zero Potential in 1-D: SSFM 28
5.7 Time Evolution in Zero Potential in 1-D: RK4IP 29
5.8 Time Evolution in Zero Potential in 2-D 30
5.9 Time Evolution in Shifted Harmonic Potential in 2-D 31
5.10 Time Evolution in Cigar-Shaped Potential in 2-D 32
5.11 Time Evolution with Interference in 2-D 34
5.12 Runtime Comparison of SSFM Vs. RK4IP 35
5.13 Runtime Comparison of Adaptive Vs. Non-Adaptive Time-Steps 36

1. Introduction

1.1 Bose-Einstein Condensates: Overview

Despite being observed only a few decades ago, the possibility of making Bose-Einstein Condensates (BECs) has been theorized many years prior to their creation [1, 2]. Having learnt about the unique properties of boson particles, Einstein predicted the existence of a state of matter that exhibits quantum mechanical effects at a macroscopic scale. In 1995, the first BEC was created using dilute alkali gases that were locally concentrated using external trapping potentials and cooled to near-zero temperatures. This forced the alkali gas particles to occupy the ground energy state of the system, thus forming a quantum mechanical object whose constituent particles all have the same momentum and are explainable by a single wave function.

This peculiar property of BECs can be used to better understand the nature of quantum mechanics at a macroscopic scale. BECs also have the potential to advance the field of quantum computing by utilizing the quantum nature of BECs to form long-lasting qubits. Given that BECs can be made from neutral atoms, they can provide greater stability as qubits relative to charged particles. Moreover, with the ever-growing precision of experimental techniques that can trap particles in potential wells, there is an increasing range of geometrical structures that can be imposed on BECs. This is likely to broaden the scenarios in which BECs can be efficiently used.

1.2 Motivation and Outline

Despite the growing feasibility of forming BECs, the process, nevertheless, remains far from being an easy task. At the same time, mere theoretical discussions are not always sufficient when trying to understand BECs. For this reason, it is necessary to develop computational tools that can model the nature and dynamics of BEC wave functions without having to construct physical condensates. To that end, the main contribution of this thesis is developing a software module in Python which implements two efficient algorithms for solving the non-linear differential equation that describes the spatial and temporal changes of BEC wave functions.

This thesis is structured as follows. Section 2 provides a brief overview of BECs and

a derivation of the Gross-Peteavskii equation used to model the dynamics of BECs. Section 3 presents two algorithms that are commonly used for solving the Gross-Peteavskii equation: the Split-Step Fourier Method (SSFM) and the Interaction Picture Fourth-Order Runge-Kutta method (RK4IP). The mathematical reasoning behind these algorithms and the motivations for using them are also discussed in Section 3. Section 4 introduces the imaginary time-step method for solving the ground state solution of the Gross-Peteavskii equation. Section 5 presents different results of simulations performed using the Python software package that is presented along with this paper. Section 6 concludes. Appendix A provides code that shows how to use the provided software package in order to recreate the simulation results in one and two dimensions.

2. Background

2.1 Bose-Einstein Condensates

A Bose-Einstein condensate (BECs) is an aggregation of a large number of particles that are all confined to the lowest quantum energy level allowed in a potential trap [3]. This grouping of a macroscopic number of particles at the same energy state allows the entire condensate to be explained by a single wave function [4]. Normally, quantum mechanics can only accurately describe the nature of very small objects, like single atoms or subatomic particles. However, BECs allow us to apply quantum mechanics at a macroscopic level.

2.1.1 Preparation

The preparation of BECs generally involves two steps [5]. The first step is to construct a potential trap in order to locally concentrate a large number of particles. There are various way to configure these traps that differ with respect to the techniques employed as well as the resulting geometry of the traps. Some of these traps include time-orbiting traps and magneto-optical traps [4]. But overall, the use of harmonic trapping potentials are commonly seen in experiments; as such, this thesis will primarily deal with the isotropic harmonic potential of the form

$$V(\vec{r}) = \frac{1}{2} m \omega_r^2 \vec{r}^2, \tag{2.1}$$

where m is mass of a single particle and ω_r is the trap frequency in the radial direction $\vec{r}$. Note that $V(\vec{r})$ is dependent on all the spatial dimensions of the system being considered: for the one-dimensional setting, $V(\vec{r}) = V(\vec{x})$; and in the two-dimensional case, $V(\vec{r}) = V(\vec{x}, \vec{y})$, and so on. Other partially symmetric harmonic traps can also be achieved by introducing aspect ratios to the potential function,

$$V(\vec{r}) = \frac{1}{2} m \omega_r^2 \sum_{i=1}^{n} \epsilon_i \vec{x_i}^2, \tag{2.2}$$

where ϵ_i dictates the relative contribution of the x_i dimension to the potential. Therefore, in the three-dimensional case, the shape of the potential trap, and, therefore, the BEC, can be modified by assigning different values to the aspect ratios ϵ_x, ϵ_y, and ϵ_z.

The next step for preparing BECs is to lower the energy of the constituent particles to the order of $\sim 0.1\mu K$ [6]. This can be achieved using a combination of multiple cooling procedures: mainly laser cooling and evaporation cooling. Laser cooling works by exposing the BEC particles to lasers that are tuned slightly below the frequency required to excite the particles' energy state. This results in only the particles moving towards the laser source being excited due to the relative increase in the laser's frequency caused by the Doppler effect. Once the excited particles return to their ground state by emitting a photon, they will experience a momentum change resulting in a force that acts in the opposite direction of the particles' motion. This procedure is very effective in reducing the temperature of the condensate particles. In addition to laser cooling, evaporation cooling can be achieved by creating a leak in the potential trap such that only high energy particles can escape the trap. This step can be repeated to further cool the system of particles and reach the critical temperature limit where all of the particles are in the ground state of the system, thus forming a BEC. This simultaneous occupation of the ground state by all particles in the system is only allowed for bosons and is strictly prohibited for fermions.

2.1.2 Pauli-Exclusion Principle

In 1925, Wolfgang Pauli formulated the Pauli-exclusion principle which states the following: for a two particle wave function, the exchange of two particles in the same state is antisymmetric for fermions and symmetric for bosons [7]. Consider the two ket vector states $|x_1\rangle$ and $|x_2\rangle$, as well as the two particle wave function $|\psi\rangle$. Then, antisymmetry under exchange is defined as

$$|\psi\rangle = \alpha_1|x_1\rangle + \alpha_2|x_2\rangle = -\left(\alpha_1|x_2\rangle + \alpha_2|x_1\rangle\right), \tag{2.3}$$

where α_1 and α_2 are complex scalar amplitudes. If the two states are identical, meaning $|x_1\rangle = |x_2\rangle$, then the asymmetry condition implies that that $\alpha_1 = -\alpha_1$ and $\alpha_2 = -\alpha_2$. This condition is only satisfied when $\alpha_1 = \alpha_2 = 0$, meaning that no two particles can have identical states if their wave function is antisymmetric under exchange. These types of particles are known as fermions.

Conversely, two bosons have a symmetric wave function under exchange:

$$|\psi\rangle = \alpha_1|x_1\rangle + \alpha_2|x_2\rangle = \alpha_1|x_2\rangle + \alpha_2|x_1\rangle, \tag{2.4}$$

which allows for identical states with non-zero probability. Since the particles that make up a BEC all share the same ground state of the system, their wavefunction must be symmetric under exchange. This is precisely why BECs can only be made using bosons and not fermions.

2.2 Gross-Pitaevskii Equation

The Gross-Pitaevskii equation (GPE) is a differential equation that can be used to describe the evolution of a BEC wave function [5]. Solving the GPE enables us to quantify the BEC wave function across time and space. The GPE arises from modifying the schrodinger

equation by accounting for the interaction potential between the constituent particles of a BEC. This modification makes the GPE more difficult to solve analytically. This is why the algorithms provided in Section 3 of this thesis are methods for numerically solving the GPE. And since the software package presented with this thesis implements these algorithms, it is fundamentally a tool for solving the GPE. Before deriving the GPE, it will be helpful to briefly summarize the fundamentals of quantum mechanics that lead to the schrodinger equation.

2.2.1 Quantum Mechanics: Review

This section provides a short recap of the building blocks of quantum mechanics. This summary closely follows the work in the introductory quantum mechanics book by Susskind [8].

State Vectors

A quantum state is represented as a vector in a complex vector space. Any state vector can be represented by a linear combination of the basis of the complex vector space. For instance, the vector space corresponding to the spin state of a particle is spanned by a linear combination of orthogonal basis vectors. Two vectors are orthogonal if there exists some measurement that can unambiguously differentiate between the two vector. In the case of the spin state vector space, the orthogonal basis vectors can be $\{|0\rangle, |1\rangle\}$, where $\{|0\rangle$ and $|1\rangle\}$ are ket vectors whose inner product is zero.

Superposition

Similar to any vector in a vector space, state vectors can be written in different basis vectors. This is known as superposition. For instance, the state $|0\rangle$ can be written in the basis $\{|-\rangle, |+\rangle\}$ as follows,

$$|0\rangle = \frac{1}{\sqrt{2}}|-\rangle + \frac{1}{\sqrt{2}}|+\rangle,$$

where,

$$|-\rangle = \frac{1}{\sqrt{2}}|0\rangle - \frac{1}{\sqrt{2}}|1\rangle,$$

and

$$|+\rangle = \frac{1}{\sqrt{2}}|0\rangle + \frac{1}{\sqrt{2}}|1\rangle.$$

Therefore, the state $|0\rangle$ is a superposition of $|-\rangle$ and $|+\rangle$; this argument extends to any n-dimensional state vector as far as a set of orthonormal basis vectors is used to express the superposition.

Measurement

A "measurable" is a hermitian operator, whose eigenvalues correspond to the possible results of a measurement. A measurable, also known as an "observable", can be represented as a matrix operator with orthonormal eigenvectors that span the vector space of the state on which the operator acts. Therefore,

$$\hat{L}|\psi\rangle = \sum_i \alpha_i |\lambda_i\rangle,$$

for some state $|\psi\rangle$ and measurable $\hat{L}$ with eigenvectors $|\lambda_i\rangle$. The coefficient α_i is the complex amplitude of the eigenvector $|\lambda_i\rangle$ and $|\alpha_i|^2$ is the probability of measuring the eigenvalue λ_i. Note that the measurement value is going to be a single eigenvalue of the measurable. This occurs due to the collapse of the superposition of $|\psi\rangle$ into one of the eigenvectors of $\hat{L}$.

Schrodinger Equation

Despite the probabilistic nature of measurements on quantum objects, the evolution of a wave function across time is nevertheless fully deterministic. The time dependence of a wave function is given by the time-dependent schrodinger equation as follows,

$$i\hbar\frac{\partial}{\partial t}\psi(\vec{r},t) = \hat{H}\psi(\vec{r},t), \tag{2.5}$$

where $\hat{H}$ is the Hamiltonian which holds information about the total energy of the system. The Hamiltonian is therefore the sum of the potential and kinetic energy of the system:

$$\hat{H} = \hat{T} + \hat{V} \tag{2.6}$$

where $\hat{V}$ is the potential operator and $\hat{T}$ is the kinetic operator.

The schrodinger equation naturally arises from the use of a time evolution operator. The state of $|\psi(t)\rangle$ at any time t can be found by acting a time evolution operator $\hat{U}(t)$ on the initial state $|\psi_0\rangle$:

$$|\psi(t)\rangle = \hat{U}(t)|\psi_0\rangle. \tag{2.7}$$

Note that this time evolution operator must be unitary such that any two initially distinct states remain distinct for all time. Now, to find a differential equation for $|\psi(t)\rangle$, we can use a differential approach for an infinitesimal time gap ε:

$$|\psi(\varepsilon)\rangle = \hat{U}(\varepsilon)|\psi_0\rangle,$$

where

$$\hat{U}(\varepsilon) = I - i\varepsilon\hat{H}$$

since $\hat{U}(\varepsilon)$ must have close to no effect when the time gap is as small as ε. So, $-i\varepsilon\hat{H}$ is the amount by which the effect of $\hat{U}(\varepsilon)$ deviates from the identity operator. Now combining the above equations gives

$$|\psi(\varepsilon)\rangle = (I - i\varepsilon\hat{H})|\psi_0\rangle,$$

$$\frac{1}{\varepsilon}\left(|\psi(\varepsilon)\rangle - |\psi_0\rangle\right) = -i\hat{H}|\psi_0\rangle.$$

Taking the limt as $\varepsilon \to 0$ in the equation above results in the schrodinger equation from Eq. (2.5), (without the $\hbar$, which is added to maintain proper dimensionality). The general solution of the schrodinger equation is

$$|\psi(t)\rangle = e^{-i\hat{H}t}|\psi_0\rangle. \tag{2.8}$$

2.2.2 GPE Derivation

The Hamiltonian used in the schrodinger equation discussed above is a one-body Hamiltonian, meaning it describes the energy of a single particle. This is because the potential function used was only dependent on the single position vector $\vec{r}$. However, in the presence of a pairwise interaction between two particles, the potential function must depend on the positions of both particles. Since the BEC constituent particles exert a small yet non-negligible force on each other, the one-body potential function $V(\vec{r})$ is modified to the two-body potential function $V(\vec{r},\vec{r}')$ by accounting for both the external trapping potential and an internal potential [9, 3]:

$$V(\vec{r},\vec{r}') = V_{ext}(\vec{r}) + V_{int}(\vec{r}-\vec{r}'), \tag{2.9}$$

where $V_{ext}(\vec{r})$ is the external trapping potential, $V_{int}(\vec{r}-\vec{r}')$ is the internal potential of the system arises from the repulsive or attractive forces between the constituent particles of the BEC, and $\vec{r}$ and $\vec{r}'$ are positions of any two particles. In the case of BECs, the interaction between particles is assumed to be non-zero when the particles are at the same location [3]. Therefore, the internal potential component can be approximated as

$$V_{int}(\vec{r}-\vec{r}') \approx g\delta(\vec{r}-\vec{r}'), \tag{2.10}$$

where g is the interaction coefficient that determines the strength of the particle-particle attraction or repulsion and is given by $g \approx 4\pi\hbar^2 a/m$; a is the s-wave scattering length of the particles; and δ is the Dirac delta which is defined as

$$\delta(x) = \begin{cases} \infty, & x = 0 \\ 0, & x \neq 0 \end{cases}, \tag{2.11}$$

and

$$\int_{-\infty}^{\infty} \delta(x)dx = 1. \tag{2.12}$$

In order to construct the Hamiltonian operator from the modified two-body potential function $V_{int}(\vec{r},\vec{r}')$, we must form an operator $\hat{V}_{int}$ that corresponds to the internal potential function. The second quantised form of this operator is

$$\hat{V}_{int} = \frac{1}{2}\int d\vec{r}\int d\vec{r}'\hat{\Psi}^\dagger(\vec{r},t)\hat{\Psi}^\dagger(\vec{r}')V_{int}(\vec{r}-\vec{r}')\hat{\Psi}(\vec{r}')\hat{\Psi}(\vec{r},t), \tag{2.13}$$

where $\hat{\Psi}(\vec{r},t)$ is a field operator, which will later be approximated to a wave function in the context of a BEC [3]. And $\hat{\Psi}^\dagger(\vec{r},t)$ is its hermitian conjugate. Substituting Eq. (2.10) into this operator gives

$$\hat{V}_{int} = \frac{1}{2}\int d\vec{r}\int d\vec{r}'\hat{\Psi}^\dagger(\vec{r},t)\hat{\Psi}^\dagger(\vec{r}')g\delta(\vec{r}-\vec{r}')\hat{\Psi}(\vec{r}')\hat{\Psi}(\vec{r},t). \tag{2.14}$$

Using the constraint on the delta function shown in Eq. (2.12), we integrate out the delta function, which yields

$$\hat{V}_{int} = \frac{g}{2}\int d\vec{r}\hat{\Psi}^\dagger(\vec{r},t)\hat{\Psi}^\dagger(\vec{r},t)\hat{\Psi}(\vec{r},t)\hat{\Psi}(\vec{r},t). \tag{2.15}$$

Therefore, the modified Hamiltonian in the second quantised form is given by

$$\hat{H} = \int d\vec{r}\hat{\Psi}(\vec{r},t)^\dagger\left(-\frac{i\hbar^2}{2m}\nabla_r^2 + \hat{V}_{ext}\right)\hat{\Psi}(\vec{r},t) + \frac{g}{2}\int d\vec{r}\hat{\Psi}^\dagger(\vec{r},t)\hat{\Psi}^\dagger(\vec{r},t)\hat{\Psi}(\vec{r},t)\hat{\Psi}(\vec{r},t), \tag{2.16}$$

where we have made the replacement

$$\hat{T} = -\frac{i\hbar^2}{2m}\nabla_r^2. \tag{2.17}$$

Recall from the Pauli-exclusion principle that bosons have symmetries that are equivalent under exchange. This is equivalent to stating

$$[\hat{\Psi}(\vec{r},t),\hat{\Psi}(\vec{r}',t)] = [\hat{\Psi}^\dagger(\vec{r},t),\hat{\Psi}^\dagger(\vec{r}',t)] = 0, \tag{2.18}$$

and

$$[\hat{\Psi}(\vec{r},t),\hat{\Psi}^\dagger(\vec{r}',t)] = \delta(\vec{r}-\vec{r}'), \tag{2.19}$$

where $[a,b] = ab - ba$. Now applying the Hamiltonian in Eq. (2.16) into the Heisenberg equation [4],

$$i\hbar\frac{\partial\hat{\Psi}(\vec{r},t)}{\partial t} = [\hat{\Psi}(\vec{r},t),\hat{H}] \tag{2.20}$$

gives the field operator version of the GPE:

$$i\hbar\frac{\partial\hat{\Psi}(\vec{r},t)}{\partial t} = \left(-\frac{i\hbar^2}{2m}\nabla_r^2 + \hat{V}_{ext} + g\hat{\Psi}^\dagger(\vec{r},t)\hat{\Psi}(\vec{r},t)\right)\hat{\Psi}(\vec{r},t). \tag{2.21}$$

This is not yet the GPE since the field operator has to be approximated to a wave function. To do so, we make the approximation that for a large number of condensate particles N,

$$\hat{\Psi}(\vec{r},t) \approx \sqrt{N}\psi(\vec{r},t) \tag{2.22}$$

In this approximation, Eq. (2.21) becomes the GPE given by

$$i\hbar\frac{\partial\psi(\vec{r},t)}{\partial t} = \left(-\frac{i\hbar^2}{2m}\nabla_r^2 + \hat{V}_{ext} + gN|\psi(\vec{r},t)|^2\right)\psi(\vec{r},t). \tag{2.23}$$

The GPE is nonlinear due to the $|\hat{\Psi}(\vec{r},t)|^2$ term introduced by the internal potential. The non-linearity of the GPE makes it difficult to analytically solve for the wave function. Therefore, the following sections of this thesis will discuss some numerical approaches for solving the GPE.

3. Numerical Approach

3.1 Setup

3.1.1 Dimensionless GPE

The GPE shown in Eq. (2.23) contains multiple constants that can be removed from the equation through non-dimensionalisation. The resulting equation will be simpler to work with both in terms of ease of understanding and reduced computational expense. To begin with, it will be helpful to explicitly state the GPE that will be used throughout the remaining sections of this thesis. Since the external trapping potential to be considered is the harmonic potential trap given in Eq. (2.2), the GPE in Eq. (2.23) becomes

$$i\frac{\partial\psi(\vec{r},t)}{\partial t} = \left(-\frac{i\hbar}{2m}\nabla_r^2 + \frac{1}{2\hbar}m\omega_r^2\sum_{i=1}^{n}\epsilon_i\vec{x_i}^2 + \frac{4\pi\hbar a}{m}N|\psi(\vec{r},t)|^2\right)\psi(\vec{r},t). \tag{3.1}$$

Therefore, the following non-dimensionalisation procedure will scale the GPE with respect to $\hbar$, m, and ω [3]. The scaling constants to be used are

$$S_l = \sqrt{\frac{\hbar}{2m\omega_r}}, \qquad \text{and} \qquad S_t = \omega_r^{-1}. \tag{3.2}$$

And the above scales result in the following non-dimensional replacements of the previous quantities:

$$\Phi \longrightarrow \hat{\Psi}{S_l}^{\frac{3}{2}} \tag{3.3}$$

$$-\frac{i\hbar}{2m}\nabla_r^2 \longrightarrow -\nabla_r^2 \tag{3.4}$$

$$\frac{1}{2}m\omega_r^2\sum_{i=1}^{n}\epsilon_i\vec{x_i}^2 \longrightarrow \frac{1}{4}\sum_{i=1}^{n}\epsilon_i\vec{\mathcal{X}_i}^2 \tag{3.5}$$

$$\frac{\vec{x_i}}{S_l} \longrightarrow \vec{\mathcal{X}}_i, \tag{3.6}$$

$$\frac{t}{S_t} \longrightarrow \tau, \tag{3.7}$$

$$\frac{a}{S_l} \longrightarrow \alpha. \tag{3.8}$$

Following the above replacements, the dimensionless GPE for a harmonic trapping potential becomes

$$i\frac{\partial\Phi(\vec{r},t)}{\partial t} = \left(-\nabla_r^2 + \frac{1}{4}\sum_{i=1}^{n}\epsilon_i\vec{\mathcal{X}}_i^{\,2} + 8\pi\alpha N|\Phi(\vec{r},t)|^2\right)\Phi(\vec{r},t). \tag{3.9}$$

From this version of the GPE, the general solution is

$$\Phi(\vec{r},t+\Delta t) = e^{-i\Delta t(\hat{T}+\hat{V})}\Phi(\vec{r},t) \tag{3.10}$$

where

$$\hat{T} = -\nabla_r^2, \tag{3.11}$$

and

$$\hat{V} = \frac{1}{4}\sum_{i=1}^{n}\epsilon_i\vec{\mathcal{X}}_i^{\,2} + 8\pi\alpha N|\Phi(\vec{r},t)|^2. \tag{3.12}$$

3.1.2 Computational Grid

The numerical solutions to be presented in the following sections require a discrete set of points in real-space, momentum-space, and time. The points in the real- and momentum-space grids are constructed by defining an array of values that corresponds to the desired number of dimensions of the GPE. On the other hand, the time grid is always a one-dimensional array of points.

Real-Space

Depending on the number of dimensions n being considered, the spatial grid is constructed from $(2M)^n$ unique points, where M is the number of Fourier modes of the grid. These spatial points are separated by Δx, which is equal across all the dimensions of the grid. Therefore,

$$x_i = \Delta x\{-M, -M+1, \ldots, M-2, M-1\} \tag{3.13}$$

where x_i is the spatial grid for the ith dimension.

Momentum-Space

The momentum-space grid consists of discrete wave numbers that are achievable in the given real-space grid. Given that the maximum length of the space grid in any dimension is $\Delta x \times 2M$, the momentum-space grid is defined as

$$k_i = \frac{2\pi}{\Delta x \times 2M}\{-M, -M+1, \ldots, M-2, M-1\} \tag{3.14}$$

where k_i is the set of wave numbers for the the ith space dimension.

Time

The temporal grid is constructed by setting initial time to be 0 and adding increments of Δt until the final desired time T is reached. The array representation of the temporal grid is

$$t = \Delta t\{0, 1, 2, \ldots, \frac{T}{\Delta t}\}. \tag{3.15}$$

The size of Δ with respect to Δx is constrained by the Hamiltonian of the GPE in Eq. (3.9). The Hamiltonian is proportional to $(\Delta x)^2$ due to the ∇_r^2 term. And, from the relation in Eq. (2.8), we require $\Delta t \ll \hat{H}$, which implies that $\Delta t \ll (\Delta x)^2$. For the simulations shown in the following sections of this thesis, we use the relation

$$\Delta t \approx \frac{(\Delta x)^2}{10}. \tag{3.16}$$

3.2 Algorithms

This thesis mainly considers two algorithms for solving the GPE. The Split-Step Fourier Method (SSFM) and the Fourth Order Runge-Kutta Interaction Picture (RK4IP). These algorithms are separately discussed in the following sections.

3.2.1 Split-Step Fourier Method

The matrix representation of the potential operator $\hat{V}$ in Eq. (3.10) has no off-diagonal components in space making its exponentiation an inexpensive operation to perform. However, the kinetic operator $\hat{T}$ is not diagonal in real-space. Therefore, $e^{\hat{T}}$ is very computationally expensive to implement. For this reason, the SSFM uses splitting approximations and Fourier transforms to provides a cost-effective way of separately performing the kinetic and potential operators on the wave function.

The operators $\hat{T}$ and $\hat{V}$ in Eq. (3.10) do not necessarily commute [10]. In other words, it is generally true that

$$[\hat{T}, \hat{V}] \neq 0. \tag{3.17}$$

Since $\hat{T}$ and $\hat{V}$ do not commute, it follows from the rule of matrix exponentiation that

$$e^{(\hat{T}+\hat{V})}\Phi(\vec{r}, t) \neq e^{\hat{T}}e^{\hat{V}}\Phi(\vec{r}, t). \tag{3.18}$$

Because of the above inequality, we must use the following approximation [4, 11]:

$$e^{-i\Delta t(\hat{T}+\hat{V})}\Phi(\vec{r}, t) \approx e^{-i\Delta t\hat{V}/2}e^{-i\Delta t\hat{T}}e^{-i\Delta t\hat{V}/2}\Phi(\vec{r}, t). \tag{3.19}$$

This approximation is second-order accurate with respect to Δt. Other more accurate approximations can be formulated with longer chains of the exponential kinetic and potential

operators [11]. However, more accurate approximations will introduce greater computational cost due to the increased number of operators involved.

As mentioned above, the kinetic operator $\hat{T}$ is not a diagonal matrix in its real-space representation. This makes its exponentiation computationally expensive. We can overcome this by diagonalizing the kinetic operator using a spectral method. This is done by representing the wave function in Fourier basis where the $e^{\nabla_r^2}$ operator is converted into a simple multiplication [12, 4].

The Fourier transform decomposes a spatially-dependent function into its constituent frequencies. The Fourier transform of $\Phi(\vec{r}, t)$ is given by

$$\mathcal{F}\{\Phi(\vec{r}, t)\} = \Theta(\vec{k}, t) = \int \Phi(\vec{r}, t) e^{i\vec{k}\vec{r}} d\vec{r} \tag{3.20}$$

where $\mathcal{F}$ represent the Fourier transformation and $\vec{k}$ is the wavevector. The corresponding inverse Fourier transform of $\Theta(\vec{k}, t)$ is given by

$$\mathcal{F}^{-1}\{\Theta(\vec{k}, t)\} = \Phi(\vec{r}, t) = (2\pi)^{-n} \int \Theta(\vec{k}, t) e^{-i\vec{k}\vec{r}} d\vec{k} \tag{3.21}$$

where $\mathcal{F}^{-1}$ represent the inverse Fourier transformation and n is the number of spatial dimensions. From the above definition, it follows that

$$\nabla_r^2 \Phi(\vec{r}, t) = \nabla_r^2 (2\pi)^{-n} \int \Theta(\vec{k}, t) e^{-i\vec{k}\vec{r}} d\vec{k}. \tag{3.22}$$

Then taking the second derivative of the right-hand side with respect to $\vec{r}$ gives

$$\nabla_r^2 \Phi(\vec{r}, t) = (2\pi)^{-n} \int -\vec{k}^2 \Theta(\vec{k}, t) e^{-i\vec{k}\vec{r}} d\vec{k}. \tag{3.23}$$

Now the definitions of $\mathcal{F}$ and $\mathcal{F}^{-1}$ into the above equation gives

$$\nabla_r^2 \Phi(\vec{r}, t) = \mathcal{F}^{-1}\{-\vec{k}^2 \mathcal{F}\{\Phi(\vec{r}, t)\}\}. \tag{3.24}$$

This shows that applying the ∇^2 operator $\Phi(\vec{r}, t)$ is equivalent to simply multiplying the Fourier representation of $\Phi(\vec{r}, t)$ by $\vec{k}$ and reverse transforming the resulting product. Now we can apply the Taylor expansion to extend Eq. (3.24) to the exponential case. From the Taylor expansion, we know that

$$e^{\nabla_r^2} = \sum_{j=0}^{\infty} \frac{\nabla_r^{2j}}{j!}. \tag{3.25}$$

Combining Eq. (3.21) and Eq. (3.25) gives

$$\begin{aligned} e^{\nabla_r^2} \Phi(\vec{r}, t) &= e^{\nabla_r^2} (2\pi)^{-n} \int \Theta(\vec{k}, t) e^{-i\vec{k}\vec{r}} d\vec{k} \\ &= \sum_{j=0}^{\infty} \frac{\nabla_r^{2j}}{j!} (2\pi)^{-n} \int \Theta(\vec{k}, t) e^{-i\vec{k}\vec{r}} d\vec{k}. \end{aligned} \tag{3.26}$$

And replacing all the ∇^2 terms with $\vec{k}$ using Eq. (3.24) results in

$$e^{\nabla_r^2}\Phi(\vec{r},t) = \mathcal{F}^{-1}\{\sum_{j=0}^{\infty}\frac{(-\vec{k}^2)^j}{j!}\mathcal{F}\{\Phi(\vec{r},t)\}\}. \tag{3.27}$$

Finally, using the Taylor expansion simplifies the above equation to

$$e^{\nabla_r^2}\Phi(\vec{r},t) = \mathcal{F}^{-1}\{e^{-\vec{k}^2}\mathcal{F}\{\Phi(\vec{r},t)\}\}. \tag{3.28}$$

This shows that the kinetic operator $\hat{T}$, which is equal to the exponential Laplacian, can be efficiently computed by first converting the wave function into Fourier basis, then multiplying by $e^{-\vec{k}^2}$, and finally reverse Fourier transforming the result. This Fourier method greatly reduces the cost of computation by removing the exponentiation of the non-diagonal Laplacean operator and replacing it with the wavevector $\vec{k}^2$.

Using the relationship in Eq. (3.28), the split approximation of $\Phi(\vec{r},t+\Delta t)$ shown in Eq. (3.19) becomes

$$\begin{aligned}\Phi(\vec{r},t+\Delta t) &= e^{-i\Delta t(\hat{T}+\hat{V})}\Phi(\vec{r},t)\\ &\approx e^{-i\Delta t\hat{V}/2}e^{-i\Delta t\hat{T}}e^{-i\Delta t\hat{V}/2}\Phi(\vec{r},t)\\ &\approx e^{-i\Delta t\hat{V}/2}\mathcal{F}^{-1}\{e^{i\Delta t\vec{k}^2}\mathcal{F}\{e^{-i\Delta t\hat{V}/2}\Phi(\vec{r},t)\}\}.\end{aligned} \tag{3.29}$$

This is the final form of the SSFM algorithm that is used to advance the wave function from $\Phi(\vec{r},t)$ to $\Phi(\vec{r},t+\Delta t)$.

3.2.2 Interaction Picture Fourth-order Runge-Kutta

Interaction Picture

As mentioned earlier, the GPE is not straightforward to solve due to the potential term which makes it a non-linear differential equation. One way to overcome this problem is by expressing GPE as a system of ordinary differential equations that are easily solvable [13]. This is achieved through a change of unknowns from $\Phi(\vec{r},t)$ to some $\zeta(\vec{r},t)$, such that

$$\frac{\partial}{\partial t}\zeta(\vec{r},t) = \alpha\zeta(\vec{r},t), \tag{3.30}$$

is an easily solvable ordinary differential equation. In order to perform the change of unknown, we apply a canonical transformation U on $\Phi(\vec{r},t)$ so that

$$\zeta(\vec{r},t)) = U(t)\Phi(\vec{r},t). \tag{3.31}$$

The operator $U(t)$ must be unitary so that the transformation is a canonical transformation, meaning it preserves the rules and mathematical structure of quantum mechanics [14]. One such transformation $U:\Phi(\vec{r},t)\rightarrow\Phi(\vec{r},t)_H$ is given by

$$U(t) = e^{it\hat{H}} \qquad \text{and} \qquad \Phi(\vec{r},t)_H = e^{it\hat{H}}\Phi(\vec{r},t). \tag{3.32}$$

Replacing $\Phi(\vec{r},t)$ with the general solution of the GPE in Eq. (3.10) reveals that the above transformation results in a time-independent picture of $\Phi(\vec{r},t)$:

$$\begin{aligned}\Phi(\vec{r},t)_H &= e^{it\hat{H}}e^{-it\hat{H}}\Phi(\vec{r},0)\\ \Phi(\vec{r},t)_H &= \Phi(\vec{r},0).\end{aligned} \tag{3.33}$$

Therefore, instead of the state vector being time dependent, the dynamics of the system is captured by the operators. This transformation of $\Phi(\vec{r},t)$ is known as the Heisenberg picture [14].

Closely related to the Heisenberg picture is the interaction picture. This picture considers the Hamiltonian H as a perturbation of a linear operator $\hat{\mathcal{D}}$ by a generally non-linear operator $\hat{\mathcal{N}}$:

$$\hat{H} = \hat{\mathcal{D}} + \hat{\mathcal{N}}. \tag{3.34}$$

In the case of the dimensionless GPE in Eq, (3.9), we have that

$$\hat{\mathcal{D}} = -\nabla_r^2, and \tag{3.35}$$

$$\hat{\mathcal{N}} = \frac{1}{4}\sum_{i=1}^{n}\epsilon_i\vec{\mathcal{X}}_i^{\,2} + 8\pi\alpha N|\Phi(\vec{r},t)|^2. \tag{3.36}$$

Given the decomposition of the Hamiltonian in Eq. (3.34), the interaction picture is equivalent to the Heisenberg picture with H being replaced by $\hat{\mathcal{D}}$:

$$\Phi(\vec{r},t)_I = e^{it\hat{\mathcal{D}}}\Phi(\vec{r},t), \tag{3.37}$$

where $\Phi(\vec{r},t)_I$ is the interaction picture of $\Phi(\vec{r},t)$. The inverse relation also holds true:

$$\Phi(\vec{r},t) = e^{-it\hat{\mathcal{D}}}\Phi(\vec{r},t)_I. \tag{3.38}$$

The schrodinger equation in the interaction picture can be found by taking the time derivative of $\Phi(\vec{r},t)_I$. Using the product rule, we get

$$\begin{aligned}\frac{\partial}{\partial t}\Phi(\vec{r},t)_I &= \frac{\partial}{\partial t}e^{it\hat{\mathcal{D}}}\Phi(\vec{r},t)\\ &= e^{it\hat{\mathcal{D}}}\hat{\mathcal{D}}\Phi(\vec{r},t) + e^{it\hat{\mathcal{D}}}\frac{\partial}{\partial t}\Phi(\vec{r},t)\\ &= e^{it\hat{\mathcal{D}}}\hat{\mathcal{D}}\Phi(\vec{r},t) + e^{it\hat{\mathcal{D}}}(-i(\hat{\mathcal{D}}+\hat{\mathcal{N}})\Phi(\vec{r},t))\\ &= -ie^{it\hat{\mathcal{D}}}\hat{\mathcal{N}}\Phi(\vec{r},t)\\ &= -ie^{it\hat{\mathcal{D}}}\hat{\mathcal{N}}e^{-it\hat{\mathcal{D}}}\Phi(\vec{r},t)_I.\end{aligned} \tag{3.39}$$

Now we can define the non-linear operator in the interaction picture $\hat{\mathcal{N}}_I$ to be [13, 3]

$$\hat{\mathcal{N}}_I(t) = e^{it\hat{\mathcal{D}}}\hat{\mathcal{N}}e^{-it\hat{\mathcal{D}}}. \tag{3.40}$$

With this definition of N_I, Eq. (3.39) becomes

$$\frac{\partial}{\partial t}\Phi(\vec{r},t)_I = -i\hat{\mathcal{N}}_I(t)\Phi(\vec{r},t)_I. \tag{3.41}$$

Observe that the above equation is an ordinary differential equation (ODE), meaning it can easily be solved using a variety of methods for solving ODEs. And once the above ODE is solved for $\Phi(\vec{r},t)_I$, then $\Phi(\vec{r},t)$ can be directly found using Eq. (3.38).

Fourth-order Runge-Kutta

Is is especially beneficial to use the fourth order Runge-Kutta (RK4) method for solving Eq. (3.41). The reason behind this particular choice of the RK4 method will be addressed in a moment. Before that, it is helpful to provide the structure of RK4 [15]. Consider the following ordinary differential equation

$$\frac{\partial x}{\partial t} = x'(x,t). \tag{3.42}$$

In the RK4 method, the time evolution of x from x_i at time t_i to x_{i+1} at time $t_i + \Delta t$ is given by

$$x_{i+1} = x_i + \frac{1}{6}(s_1 + 2(s_2 + s_3) + s_4), \tag{3.43}$$

where

$$s_1 = \Delta t x'\left(x_i, t_i\right) \tag{3.44}$$

$$s_2 = \Delta t x'\left(x_i + \frac{s_1}{2}, t_i + \frac{\Delta t}{2}\right) \tag{3.45}$$

$$s_3 = \Delta t x'\left(x_i + \frac{s_2}{2}, t_i + \frac{\Delta t}{2}\right) \tag{3.46}$$

$$s_4 = \Delta t x'\left(x_i + \frac{s_3}{2}, t_i + \Delta t\right). \tag{3.47}$$

To utilize the special properties of RK4, we will set an arbitrary time t' as the time when the interaction picture is the same as the normal (schrodinger) picture [14, 13]. At time t',

$$\Phi(\vec{r},t')_I = \Phi(\vec{r},t'). \tag{3.48}$$

This modifies the interaction picture transformation in Eq. (3.37) to

$$\Phi(\vec{r},t)_I = e^{i(t-t')\hat{\mathcal{D}}}\Phi(\vec{r},t), \tag{3.49}$$

and the non-linear operator $\hat{\mathcal{N}}_I$ becomes

$$\hat{\mathcal{N}}_I(t) = e^{i(t-t')\hat{\mathcal{D}}}\hat{\mathcal{N}}e^{-i(t-t')\hat{\mathcal{D}}}. \tag{3.50}$$

With these changes made, the time evolution of the wave function in the interaction picture $\Phi(\vec{r})_I$ from $\Phi(\vec{r})_i^I$ at time t_i to $\Phi(\vec{r})_{i+1}^I$ at time $t_i + \Delta t$ is given by

$$\Phi(\vec{r})_{i+1}^I = \Phi(\vec{r})_i^I + \frac{1}{6}(s_1 + 2(s_2 + s_3) + s_4), \tag{3.51}$$

where

$$s_1 = -i\Delta t\hat{\mathcal{N}}_I\left(t_i\right)\Phi(\vec{r})_i^I \tag{3.52}$$

$$s_2 = -i\Delta t\hat{\mathcal{N}}_I\left(t_i + \frac{\Delta t}{2}\right)\left(\Phi(\vec{r})_i^I + \frac{s_1}{2}\right) \tag{3.53}$$

$$s_3 = -i\Delta t\hat{\mathcal{N}}_I\left(t_i + \frac{\Delta t}{2}\right)\left(\Phi(\vec{r})_i^I + \frac{s_2}{2}\right) \tag{3.54}$$

$$s_4 = -i\Delta t\hat{\mathcal{N}}_I\left(t_i + \Delta t\right)\left(\Phi(\vec{r})_i^I + s_3\right). \tag{3.55}$$

The reason for selecting RK4 is that we can set $t' = t_i + \Delta t/2$ for each application of the RK4 in order to reduce the number of computations [13, 16]. This eliminates the terms $e^{i(t-t')\hat{\mathcal{D}}}$ and $e^{-i(t-t')\hat{\mathcal{D}}}$ from the interaction picture of the potential term $\hat{\mathcal{N}}_I(t)$ in s_2 and s_3. Therefore, the RK4 method with $t' = t_i + \Delta t/2$ will have the following coefficients for s_2 and s_3:

$$s_2 = -i\Delta t\hat{\mathcal{N}}\left(t_i + \frac{\Delta t}{2}\right)\left(\Phi(\vec{r})_i^I + \frac{s_1}{2}\right) \tag{3.56}$$

$$s_3 = -i\Delta t\hat{\mathcal{N}}\left(t_i + \frac{\Delta t}{2}\right)\left(\Phi(\vec{r})_i^I + \frac{s_2}{2}\right) \tag{3.57}$$

Thus, setting $t' = t_i + \Delta t/2$ reduces the computational cost of performing the RK4 method on the interaction picture of the wave function. Now using the relation between $\Phi(\vec{r}, t)$ and $\Phi(\vec{r}, t)_I$ in Eq. (3.38) and the definition of $\hat{\mathcal{N}}_I(t)$ in Eq. (3.50), the full RK4IP algorithm for finding the time evolution of $\Phi(\vec{r}, t)$ from $\Phi(\vec{r})_i$ at time t_i to $\Phi(\vec{r})_{i+1}$ at time $t_i + \Delta t$ is given by

$$\Phi(\vec{r})_{i+1} = e^{-i(\Delta t/2)\hat{\mathcal{D}}}\Phi(\vec{r})_{i+1}^I, \tag{3.58}$$

$$\Phi(\vec{r})_{i+1}^I = \Phi(\vec{r})_i^I + \frac{1}{6}(s_1 + 2(s_2 + s_3) + s_4), \tag{3.59}$$

$$s_1 = e^{i(\Delta t/2)\hat{\mathcal{D}}}\left(-i\Delta t\hat{\mathcal{N}}\left(t_i\right)\right)e^{-i(\Delta t/2)\hat{\mathcal{D}}}\Phi(\vec{r})_i^I \tag{3.60}$$

$$s_2 = -i\Delta t\hat{\mathcal{N}}\left(t_i + \frac{\Delta t}{2}\right)\left(\Phi(\vec{r})_i^I + \frac{s_1}{2}\right) \tag{3.61}$$

$$s_3 = -i\Delta t\hat{\mathcal{N}}\left(t_i + \frac{\Delta t}{2}\right)\left(\Phi(\vec{r})_i^I + \frac{s_2}{2}\right) \tag{3.62}$$

$$s_4 = e^{i(\Delta t/2)\hat{\mathcal{D}}}\left(-i\Delta t\hat{\mathcal{N}}\left(t_i + \Delta t\right)\right)e^{-i(\Delta t/2)\hat{\mathcal{D}}}\left(\Phi(\vec{r})_i^I + s_3\right). \tag{3.63}$$

Note that all exponentiation of $\hat{\mathcal{D}}$ is replaced using the Fourier method given in Eq. (3.28). This is the final form of the RK4IP algorithm that is used to advance the wave function from $\Phi(\vec{r}, t)$ to $\Phi(\vec{r}, t + \Delta t)$.

3.2.3 Adaptive Time-Step

As with any time-stepping algorithm, the ones discussed in this paper use a predetermined value of Δt to evolve a function across time. This approach however relies on the correct choice of Δt being made such that the time evolution remains stable. Although an upper bound for Δt is suggested in Eq. (3.16), it is generally more difficult to find the proper Δt for the given parameters of the GPE. Therefore, along with the implementation of the algorithms discussed above, this paper also adds the option to use an adaptive time-step [17].

The adaptive time-step procedure allows for the time-step value to vary from its initial value. When the adaptive time-step option is enabled, the proper Δt is identified for each execution of the SSFM or the RK4IP. This is done by embedding the same time-stepping algorithm that evolves the function by taking two half time-steps instead of one full time-step. The difference between a double half-time step and a single full time-step evolution will determine the error associated with using Δt instead of $\Delta t/2$.

The decision to switch from a larger to a smaller time-step is made using an error tolerance range. If the difference in the result of the wave function from using a large time-step instead of a small time-step is within the error tolerance range, then the larger time-step is maintained. However, if the difference falls above the upper bound of the error tolerance, then the smaller time-step will be chosen over the larger one. Lastly, if the difference falls below the lower bound of the error tolerance, it means there is very little difference between using either time-step. Therefore, a new time-step equal to twice the larger time-step will be used. As shown in Fig. (5.13), the adaptive time-step greatly reduces the time taken to complete a given number of iterations that have to be taken to evolve the wave function towards a desired time.

4. Ground State Solution

The python package developed alongside this paper provides two main functionalities. The first is to find the ground state wave function solution of the GPE using an imaginary time-step algorithm. The second is to evolve the ground state function across time. Given that a BEC is prepared with all of its constituent particles being in the ground state, finding the ground state wave function of the BEC is a necessary step before any time evolution can be performed. However, during the time evolution of the wave function, no change in the probability density distribution of the wave function will be observed unless there is a change in the Hamiltonian of the system. This change is introduced by removing or modifying the external potential trap of the system.

4.1 Guessing Initial Wave Function

In order to solve for the ground state wave function of the BEC, we first make a guess of what the ground state would look like. In the implemented code, this guess assumes the external potential trap configuration to have the form of an isotropic harmonic oscillator shown in Eq. (2.1). Using this assumption, the initial guess is made using the Thomas-Fermi approximation [3]

$$|\eta(\vec{r},t)|^2 = \frac{V(\vec{r})}{g}\left(1-\frac{\vec{r}^2}{R^2}\right), \tag{4.1}$$

where $\eta(\vec{r},t)$ is the guessed ground state wave function, $V(\vec{r})$ is the sum of the external and internal potential, g is the interaction coefficient of the internal potential and $R^2 = 2V(\vec{r})/(m\omega_r^2)$. Note that for the sake of clarity, the above expression is not dimensionless. The next step to solving the true ground state solution is to evolve the guessed ground state in imaginary time.

4.2 Imaginary Time Evolution

Imaginary time propagation is a numerical method for evolving a function across imaginary time τ where $\tau = -it$ [3]. This method can be used to solve the ground state solution using the guessed solution. Recall that a given wave function can be expressed as combination

of time-independent energy eignestates and time-dependent amplitudes: in the case of the guessed function,

$$\eta(\vec{r},t) = \sum_j \alpha_j(t)\lambda_j(\vec{r}), \tag{4.2}$$

where $\lambda_j(\vec{r})$ is the jth energy eigenstate associated with the energy eigenvalue E_j and $\alpha_j(t)$ is the corresponding complex coefficient of the eigenstate. Using the schrodinger equation in Eq. (2.8), the time evolution of $\eta(\vec{r},t)$ from time t to time $t+\Delta t$ is given by

$$\begin{aligned}\eta(\vec{r},t+\Delta t) &= e^{-i\Delta t H}\eta(\vec{r},t) \\ &= \sum_j e^{-i\Delta t E_j}\alpha_j(t)\lambda_j(\vec{r}).\end{aligned} \tag{4.3}$$

Now, making the substitution from regular time t to imaginary time $\tau = -it$ modifies the above equation as follows:

$$\eta(\vec{r},\tau+\Delta\tau) = \sum_j e^{-\Delta\tau E_j}\alpha_j(\tau)\lambda_j(\vec{r}). \tag{4.4}$$

Due to the negative coefficient attached to the energy egenvalue E_j, a step forward in imaginary time multiplies the coefficient of each eigenstate with a value less than one, thereby reducing the magnitude of the initial wave function. But notice that the eigenstates corresponding to larger energy eigenvalues experience greater decay compared to those with smaller energy eigenvalues. In other words, for an ordered set of eigenvalues $E_0 < E_1 < \ldots < E_n$,

$$\left|\frac{d}{d\tau}e^{-\tau E_0}\right| < \left|\frac{d}{d\tau}e^{-\tau E_1}\right| < \ldots < \left|\frac{d}{d\tau}e^{-\tau E_n}\right|. \tag{4.5}$$

And since the wave function corresponds to the smallest energy eigenvalue, its coefficient will have the slowest decay. Now if we normalize the wave function after each forward step in imaginary time, the new wave function at imaginary time $\tau+\Delta\tau$ will contain a greater proportion of smaller eigenstates relative to the previous wave function at imaginary time τ. Therefore, as we continue evolving $\eta(\vec{r},\tau)$ in imaginary time using the Hamiltonain H for the BEC system, the wave function will eventually only consist of the eingenstate of H corresponding to the smallest energy eigenvalue:

$$\lim_{\tau\to\infty}\eta(\vec{r},\tau+\Delta\tau) = e^{-\Delta\tau E_0}\eta(\vec{r},\tau). \tag{4.6}$$

Therefore the ground state solution of $\Phi(\vec{r},t)$ represented by $\Phi(\vec{r})_0$ will be

$$\lim_{\tau\to\infty}\eta(\vec{r},\tau) = \Phi(\vec{r})_0. \tag{4.7}$$

Of course, this approach of indefinitely evolving $\eta(\vec{r},\tau)$ to infinity is not a viable computational option. Therefore, we can track to the convergence of the dominant energy eigenvalue

towards the ground energy eigenvalue and terminate the imaginary time evolution once a desirable level of congruence is attained. To do this, we first express the ground state energy E_0 by taking the logarithm of both sides of Eq. (4.6), which gives

$$\lim_{\tau\to\infty} E_0 = \frac{1}{\Delta\tau} \ln\left(\frac{\eta(\vec{r},\tau)}{\eta(\vec{r},\tau+\Delta\tau)}\right). \tag{4.8}$$

Since E_0 is time-independent, we also get

$$\lim_{\tau\to\infty} \frac{d}{d\tau} E_0 = \frac{d}{d\tau}\left(\frac{1}{\Delta\tau} \ln\left(\frac{\eta(\vec{r},\tau)}{\eta(\vec{r},\tau+\Delta\tau)}\right)\right) = 0 \tag{4.9}$$

The term inside the derivative in the right-hand side of the equation is approximated using the difference between two successive steps in the time evolution. Again, this relation is only true in the limit of infinity. Therefore, we can set some error threshold ϵ so that we terminate the imaginary time evolution at time τ_f which is when

$$\frac{d}{d\tau}\left(\frac{1}{\Delta\tau} \ln\left(\frac{\eta(\vec{r},\tau_f)}{\eta(\vec{r},\tau_f+\Delta\tau)}\right)\right) = \epsilon. \tag{4.10}$$

This condition ensures the wave function at imaginary time τ_f is close to the the ground state solution of $\Phi(\vec{r},t)$. Therefore, we can modify Eq. (4.7) into a computationally calculable version:

$$\eta(\vec{r},\tau_f) \approx \Phi(\vec{r})_0. \tag{4.11}$$

The imaginary time-step algorithm discussed in this section is implemented in the python package provided with this thesis. The implementation uses the SSFM method discussed in Section 3.2.1 with a few modifications. The first modification is the substitution $t \to -it$. The second modification comes from normalizing the wave function after each step in imaginary time.

5. Simulations

This section presents different results of simulations performed using the Python software package that is presented along with this paper. These simulations mainly visualize the process of finding the ground state solution as well as the time evolution of the ground state that is triggered by a change in the external trapping potential. Unless stated otherwise, the following simulations are based on the dimensionless version of the GPE in Eq. (3.9). Therefore, the only relevant parameters are the spatial step-size Δx, temporal step-size Δt, number of time-step progressions N_t, scattering length α, number of particles N, half the number of Fourier modes M, and the ground state convergence error ϵ. Recall that M is used to determine the spatial grid as shown in Eq. (3.13) and α determines the strength of the interaction between the BEC constituents. Note that all of the simulations below are considered to be in dimensionless units.

5.1 Finding the Ground State

Here, we present the results from using the imaginary time-step algorithm to find the ground state of a wave function subject to a specified Hamiltonian. As mentioned in Section (4.1), the initial step to solving for the ground state of $\Phi(\vec{r}, t)$ is to initialize a guess wave function based on the Hamiltonian. This guess is then evolved in imaginary time until the ground state solution in reached.

5.1.1 Examples in 1-D

The result shown in Fig. (5.1) is the probability density distribution of a guessed wave function with the external potential trap being a harmonic oscillator. Note that although the Thomas-Fermi approximation in Eq. (4.1) is stated in dimensional units, all of the simulations below are in dimensionless units.

Fig. (5.2) compares the probability density distribution of the guessed function from Fig. (5.1) with that of the ground state solution that is acquired using imaginary time evolution. As mentioned earlier, the difference in the dominant energy eigenvalue between two successive imaginary time steps is used to determine the convergence of the guessed wave function towards the ground state solution of the GPE.

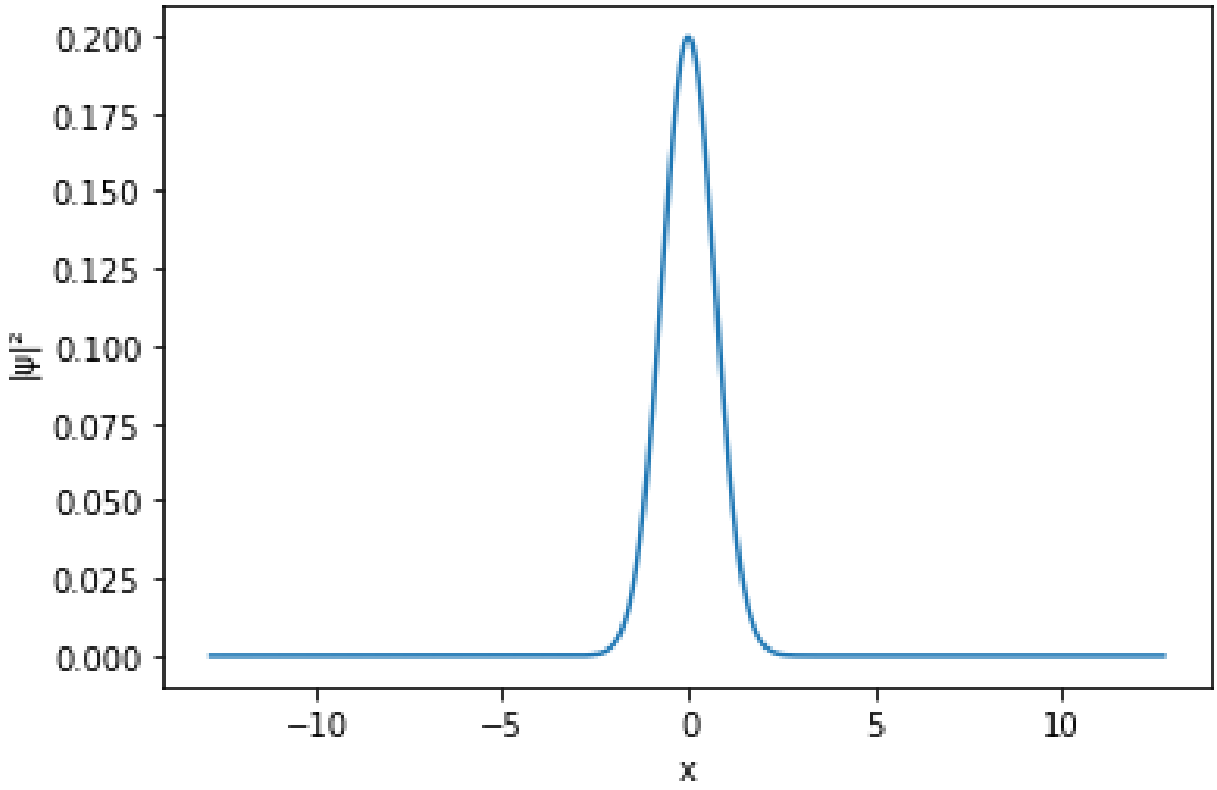

Figure 5.1: Guessed Wave Function in 1-D
Parameters: $\Delta x = 0.05$, $\Delta t = \Delta x^2/10$, $N = 2000$, $\alpha = 0.006$, $M = 2^8$, and $V(\vec{x}) = \frac{x^2}{2}$.

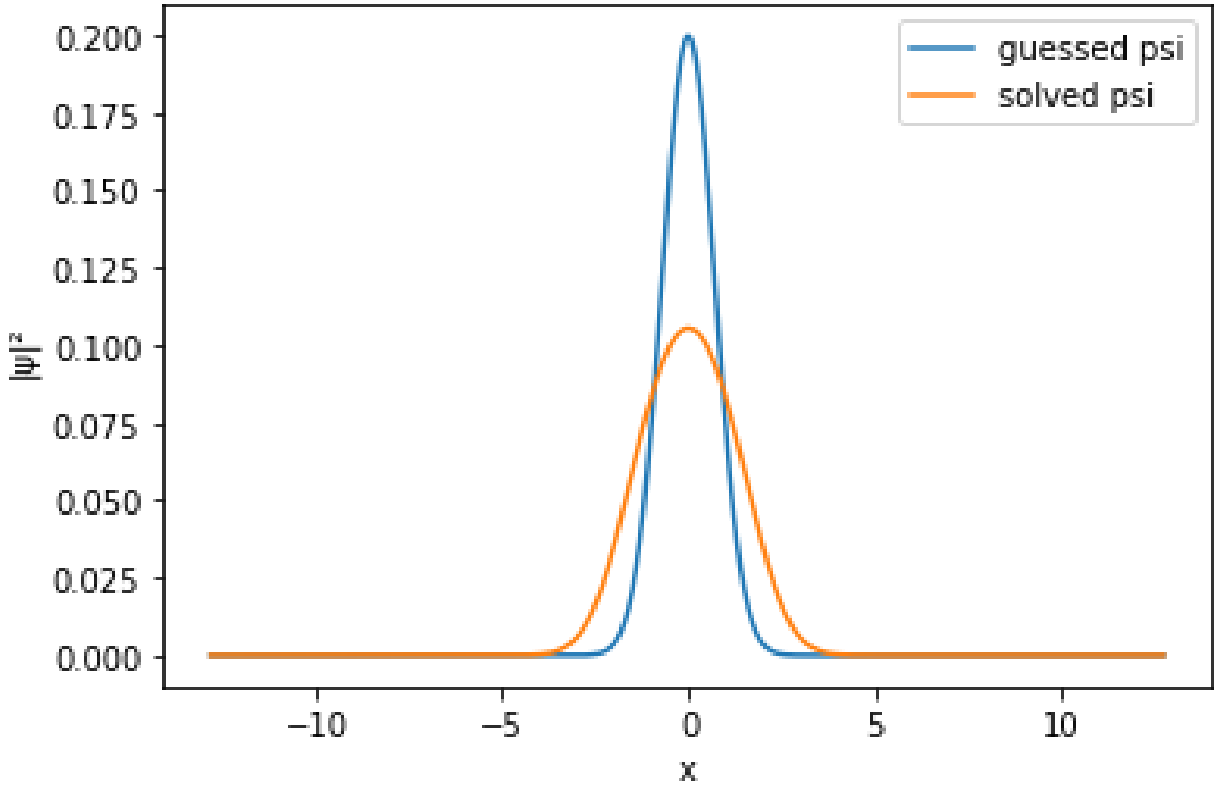

Figure 5.2: Guessed Vs. Ground Wave Function in 1-D
Parameters: $\Delta x = 0.05$, $\Delta t = \Delta x^2/10$, $N = 2000$, $\alpha = 0.006$, $M = 2^8$, $\epsilon = 10^{-5}$, and $V(\vec{x}) = \frac{x^2}{2}$.

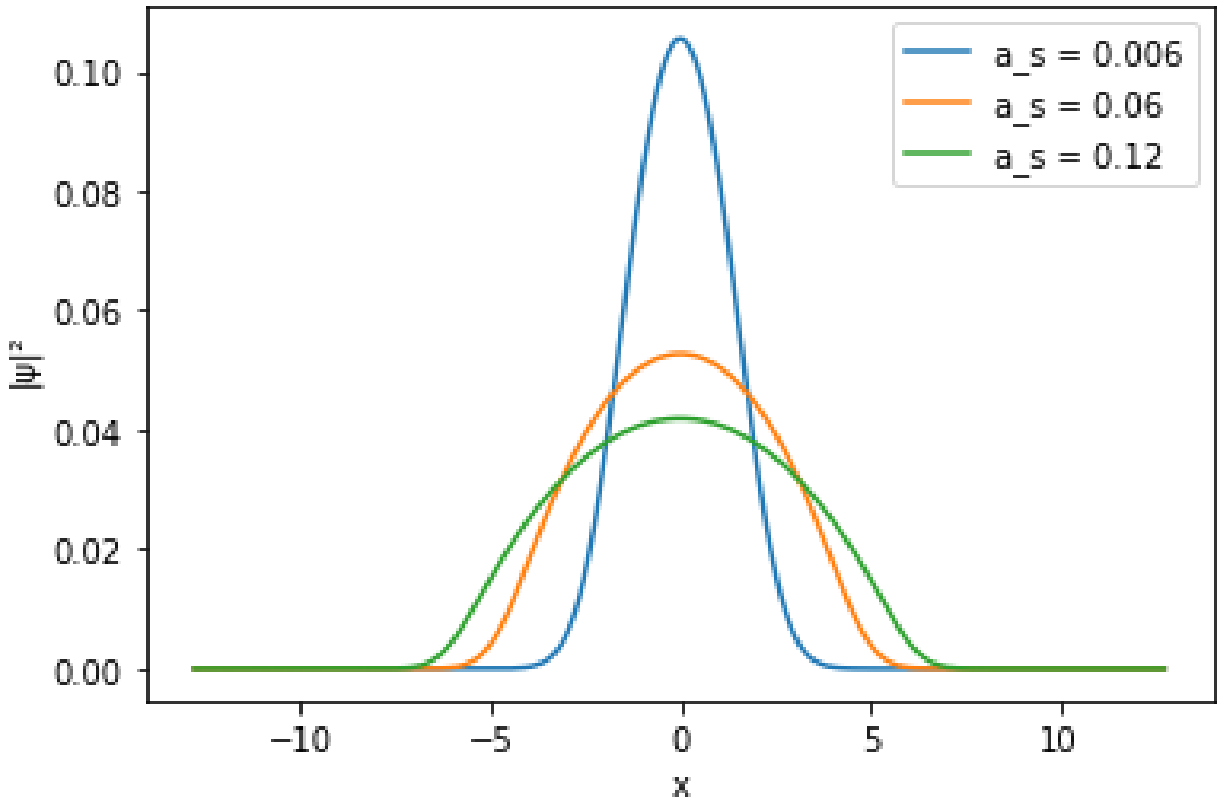

Figure 5.3: Ground States Comparison in 1-D
Parameters: $\Delta x = 0.05$, $\Delta t = \Delta x^2/10$, $N = 2000$, $\alpha_1 = 0.006$, $\alpha_2 = 0.06$, $\alpha_3 = 0.12$, $M = 2^8$, $\epsilon = 10^{-5}$, and $V(\vec{x}) = \frac{x^2}{2}$.

Fig. (5.3) shows the effect of increasing the scattering length of particles on the shape of the ground state solution. From Eq. (2.10), we know that a larger scattering length results in a stronger interaction potential among the BEC constituent particles, which leads to a more spread out probability density distribution. This effect is observed in Fig. (5.3) as the probability densities corresponding to higher scattering lengths have relatively shorter peaks and are more spread out.

5.1.2 Example in 2-D

The two-dimensional versions of the guessed wave function and the solved ground wave function from Fig. (5.2) are shown in Fig. (5.4) and Fig. (5.5), respectively.

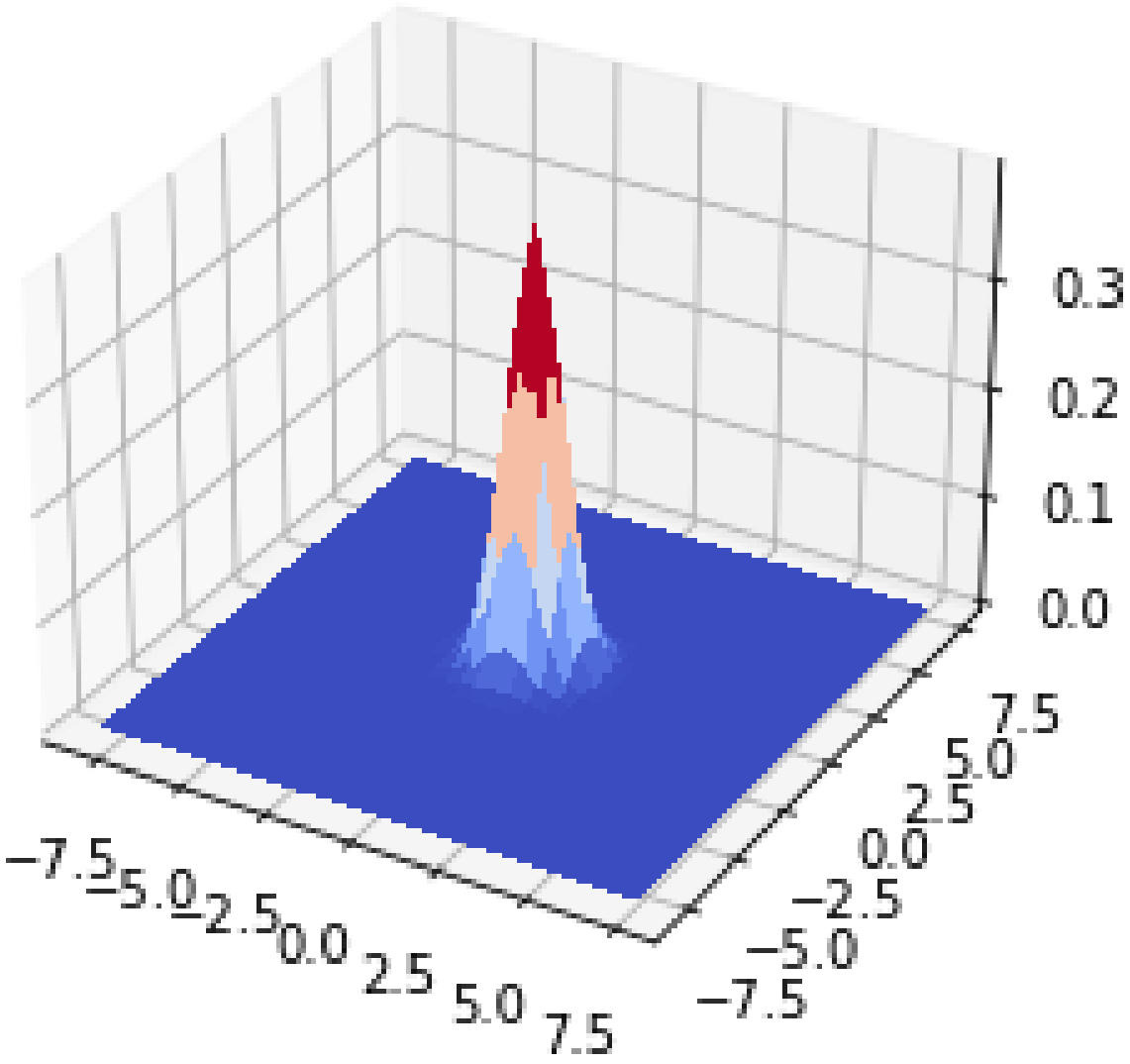

Figure 5.4: Guessed Wave Function in 2-D
Parameters: $\Delta x = 0.5$, $\Delta t = \Delta x^2/10$, $N = 2000$, $\alpha = 0.006$, $M = 2^4$, $\epsilon = 10^{-5}$, and $V(\vec{r}) = \frac{1}{2}(\vec{x}^2 + \vec{y}^2)$.

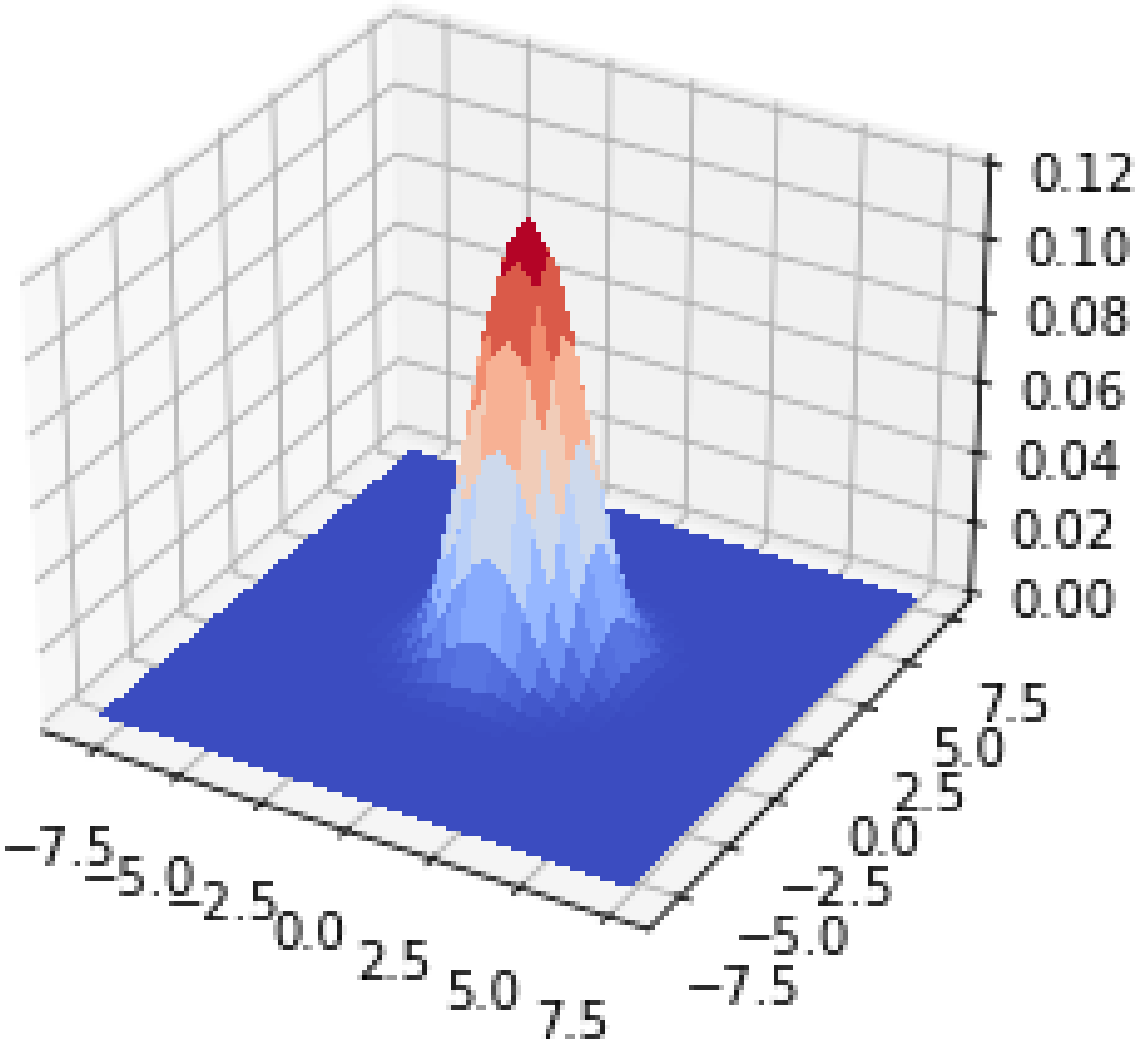

Figure 5.5: Guessed Vs Ground Wave Function in 2-D
Parameters: $\Delta x = 0.5$, $\Delta t = \Delta x^2/10$, $N = 2000$, $\alpha = 0.006$, $M = 2^8$, $\epsilon = 10^{-5}$, and $V(\vec{r}) = \frac{1}{2}(\vec{x}^2 + \vec{y}^2)$.

5.2 Time Evolution

Once the ground state solution in found, either the SSFM or the RK4IP algorithms can be used to evolve the ground state across time. For any change in the magnitude of the wave function to be observed throughout the time evolution, the external potential must either be removed or changed. This is because the time dependence of the ground state wave function only exists as a phase change, which has no effect on its probability density. However, when the external trapping potential is altered, the ground state wave function will no longer be an eigenstate of the Hamiltonian since the Hamiltonian changes as a consequence of the alteration to the external trapping potential.

5.2.1 Example in 1-D

Fig. (5.6) shows the time evolution of the ground state wave function after the external potential is fully removed. This time evolution is performed used the SSFM for stepping forward in time. As shown in the figure, in the absence of an external trapping potential, the internal potential of the BEC forces the probability density distribution to expand in space. As expected, the peaks of the probability density distribution become weaker across time. Fig. (5.7) shows the same time evolution performed with the RK4IP method. From comparing Fig. (5.6) and Fig. (5.7), we can see that both methods of time evolution result in the same outcome.

5.2.2 Examples in 2-D

Fig. (5.8) is the two-dimensional version of Fig. (5.7), where the time evolution of the ground state wave function is observed after the external potential is fully removed. Similar to the one-dimensional case, the expected result is observed. The probability density distribution spreads out in space due to the internal potential of the BEC.

Fig. (5.9) shows the time evolution of the ground state after the initial potential trap is shifted in space by some amount. Since this shift changes the position of the lowest potential point in the harmonic oscillator, it consequently causes the ground wave function to be at a higher potential. Much like a mass being released into a high potential point of a harmonic oscillator, the wave function undergoes an oscillation towards and away from the lowest point of the new potential trap.

Fig. (5.10) shows the effect of a different change in the initial potential trap where the region of least potential remains at the center but the aspect ratios are changed such that $\epsilon_y = \epsilon_z \neq \epsilon_x$. Due to this change in the shape of the potential distribution, the wave function once again undergoes an oscillatory movement where the peak remains stationary while the rest of the distribution oscillates between expansion and contraction.

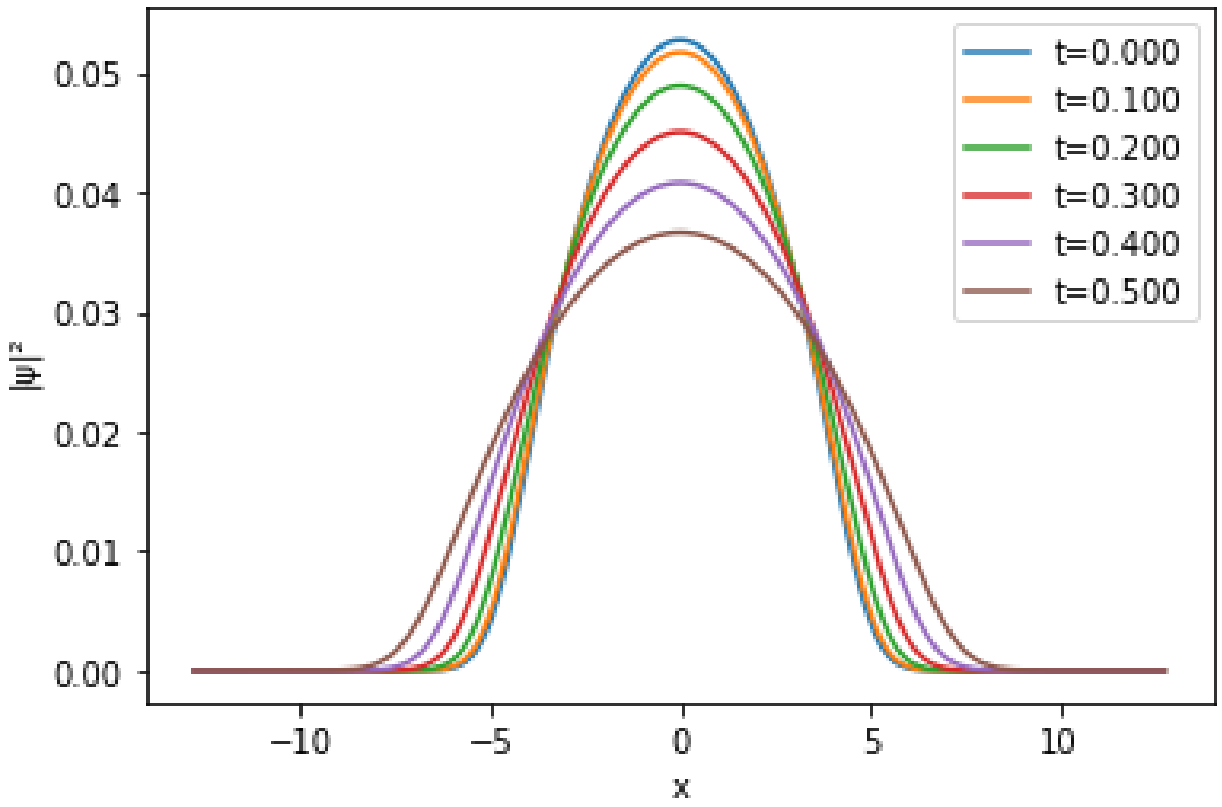

Figure 5.6: Time Evolution in Zero Potential in 1-D: SSFM
Parameters: $\Delta x = 0.05$, $\Delta t = \Delta x^2/10$, $N_t = 2000$, $N = 2000$, $\alpha = 0.006$, $M = 2^8$, $\epsilon = 10^{-5}$, stepper method = SSFM, and $V(\vec{x}) = 0$.

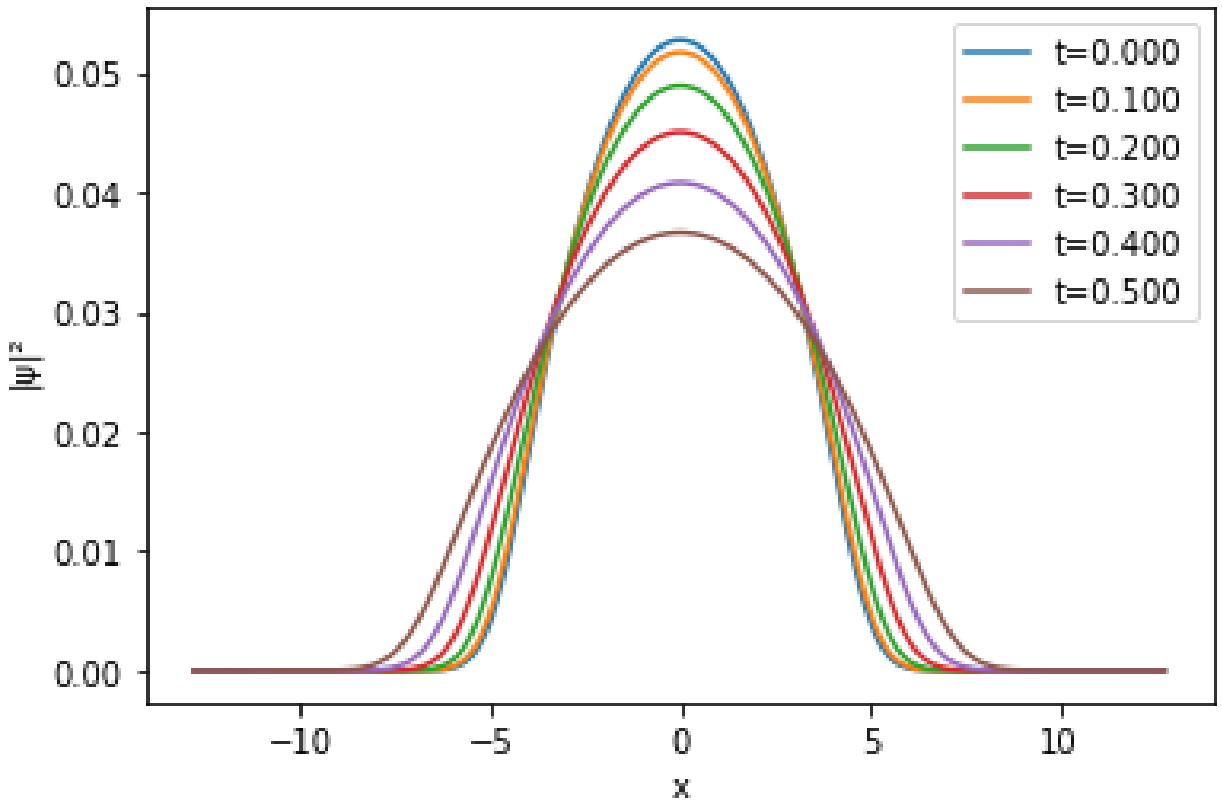

Figure 5.7: Time Evolution in Zero Potential in 1-D: RK4IP
Parameters: $\Delta x = 0.05$, $\Delta t = \Delta x^2/10$, $N_t = 2000$, $N = 2000$, $\alpha = 0.006$, $M = 2^8$, $\epsilon = 10^{-5}$, stepper method = RK4IP, and $V(\vec{x}) = 0$.

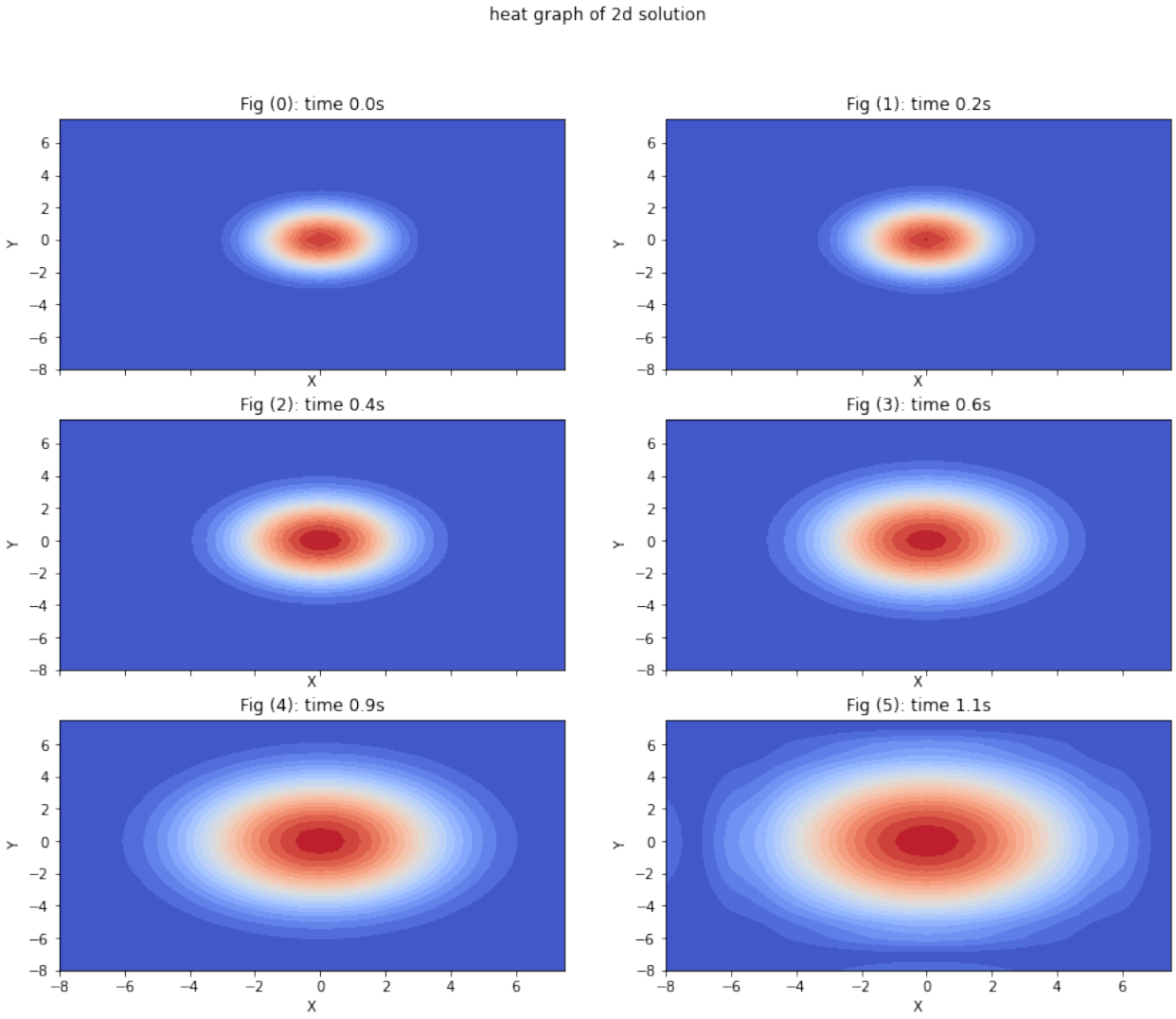

Figure 5.8: Time Evolution in Zero Potential in 2-D
Parameters: $\Delta x = 0.5$, $\Delta t = \Delta x^2/35$, $N = 2000$, $\alpha = 0.006$, $M = 2^4$, $\epsilon = 10^{-5}$, stepper method = RK4IP, $N_t = 200$, and $V(\vec{r}) = 0$.

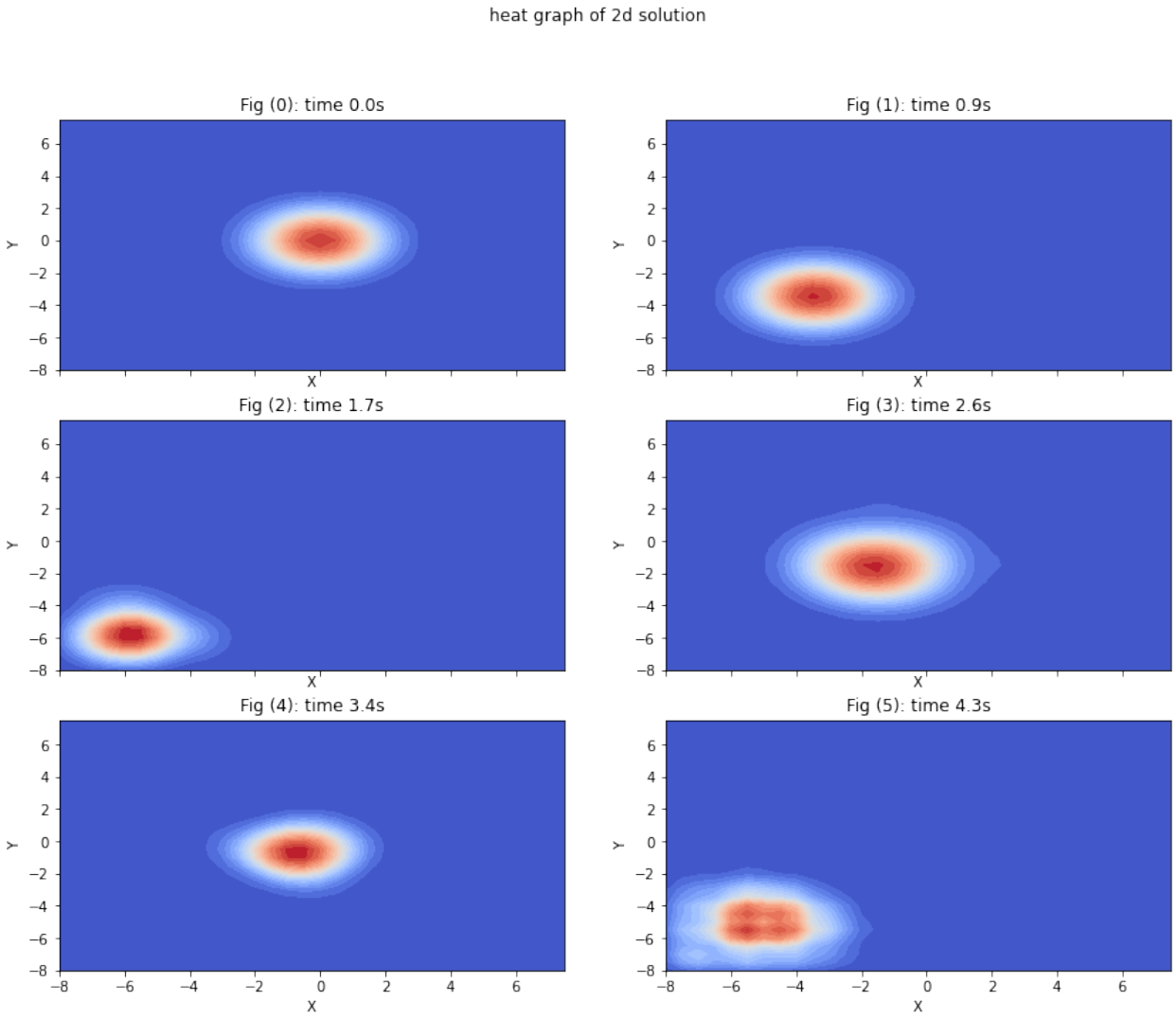

Figure 5.9: Time Evolution in Shifted Harmonic Potential in 2-D
Parameters: $\Delta x = 0.5$, $\Delta t = \Delta x^2/35$, $N = 2000$, $\alpha = 0.006$, $M = 2^4$, $\epsilon = 10^{-5}$, stepper method = RK4IP, $N_t = 800$, and $V(\vec{r}) = \frac{1}{2}((\vec{x}+3)^2 + (\vec{y}+3)^2)$.

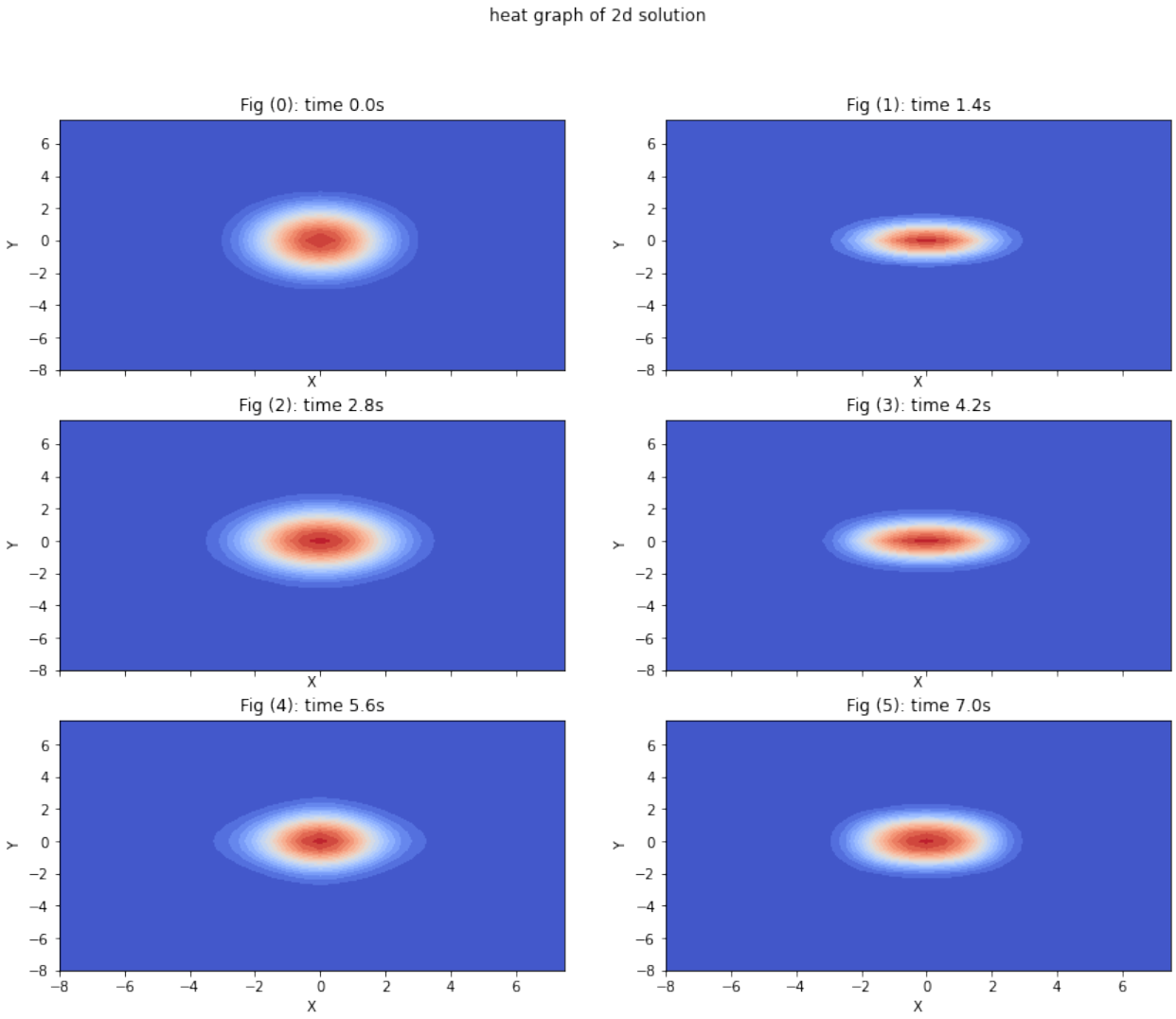

Figure 5.10: Time Evolution in Cigar-Shaped Potential in 2-D
Parameters: $\Delta x = 0.5$, $\Delta t = \Delta x^2/35$, $N = 2000$, $\alpha = 0.006$, $M = 2^4$, $\epsilon = 10^{-5}$, stepper method = RK4IP, $N_t = 1300$, and $V(\vec{r}) = \frac{1}{2}(\vec{x}^2 + 3\vec{y}^2)$.

5.3 Interference

The previous section showed the use of the time evolution algorithms to propagate the ground state wave function across time. Till now, this involved only one wave function. Therefore, a natural extension of this approach is the time evolution of multiple interfering wave functions. This can easily be achieved by first summing each of the wave functions being considered and evolving their sum across time. This process can be useful when dealing with multiple closely localized BECs being released from their potential traps.

5.3.1 Example in 2-D

Fig. (5.11) shows the time evolution of the interference of two BEC wave functions that are fully released from their potential trap.

5.4 Performance Comparison

Let's begin with a brief comparison of the runtime of the two algorithms discussed in this paper: RK4IP and SSFM. The main source of difference in the runtime between the two algorithms comes from the the number of Fourier transforms being used. This is because multidimensional Fourier transformation take up most of the computational cost of the two algorithms. Evidently, the RK4IP method uses more Fourier transforms and is therefore slower to execute relative to the SSFM. This is shown in Fig. (5.12). As the number of iterations increases, the runtime of the RK4IP method increases faster than that of the SSFM.

There is also a significant difference in the rumntime between the adaptive and non-adaptive time-step implementations of each algorithm. As expected, the adaptive time-step algorithm has a significant reductions in runtime for implementations with time-step values that are initially too small. By increasing the time-step whenever the cost of doing so is within the tolerance limit, the adaptive time-step implementation achieves a much smaller runtime. This is seen in Fig. (5.13), which shows that the adaptive time-step aproach has a significantly smaller runtime compared to the non-adaptive case.

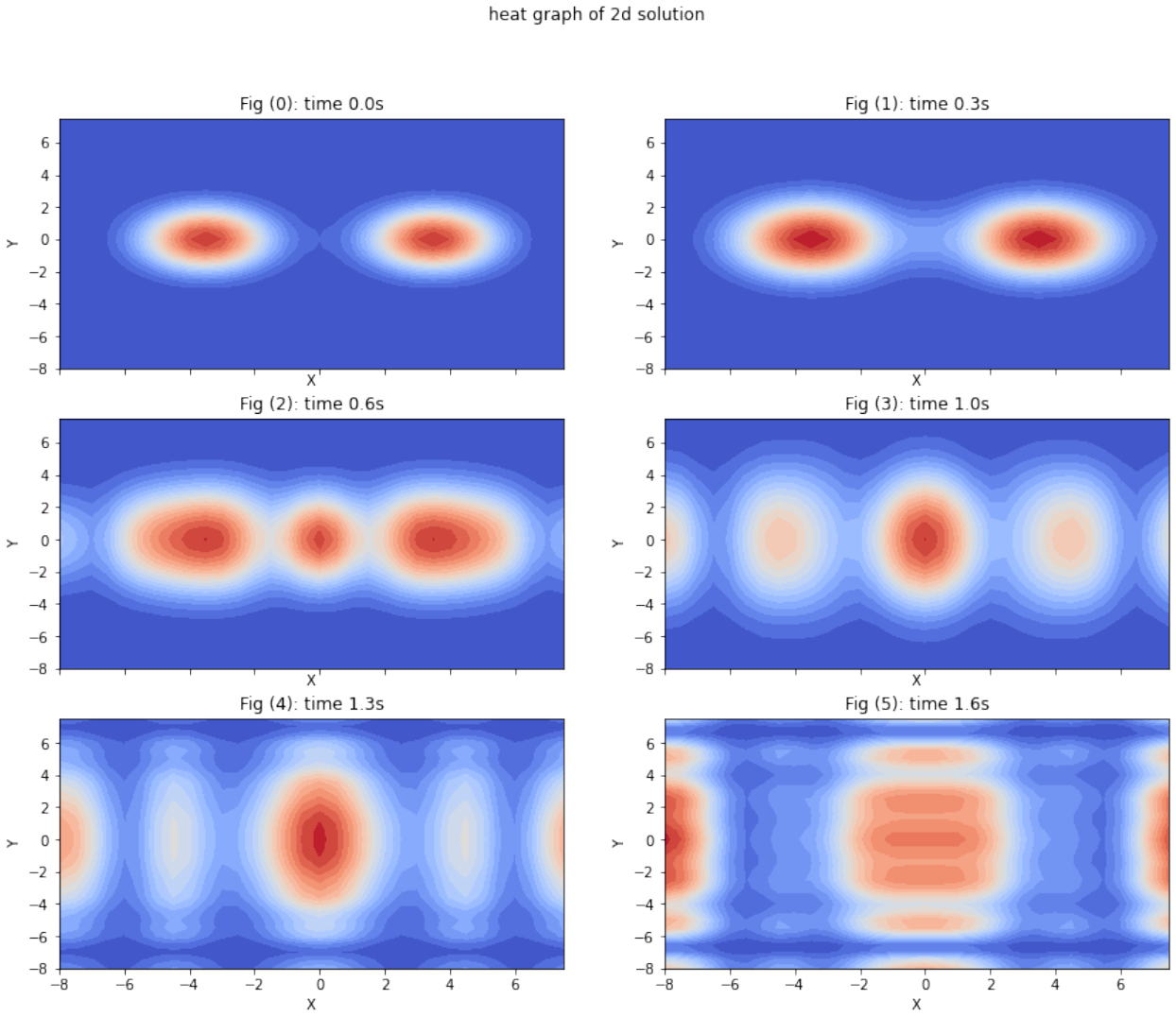

Figure 5.11: Time Evolution with Interference in 2-D
Parameters: $\Delta x = 0.5$, $\Delta t = \Delta x^2/35$, $N = 2000$, $\alpha = 0.006$, $M = 2^4$, $\epsilon = 10^{-5}$, stepper method = RK4IP, $N_t = 250$, and $V(\vec{r}) = 0$.

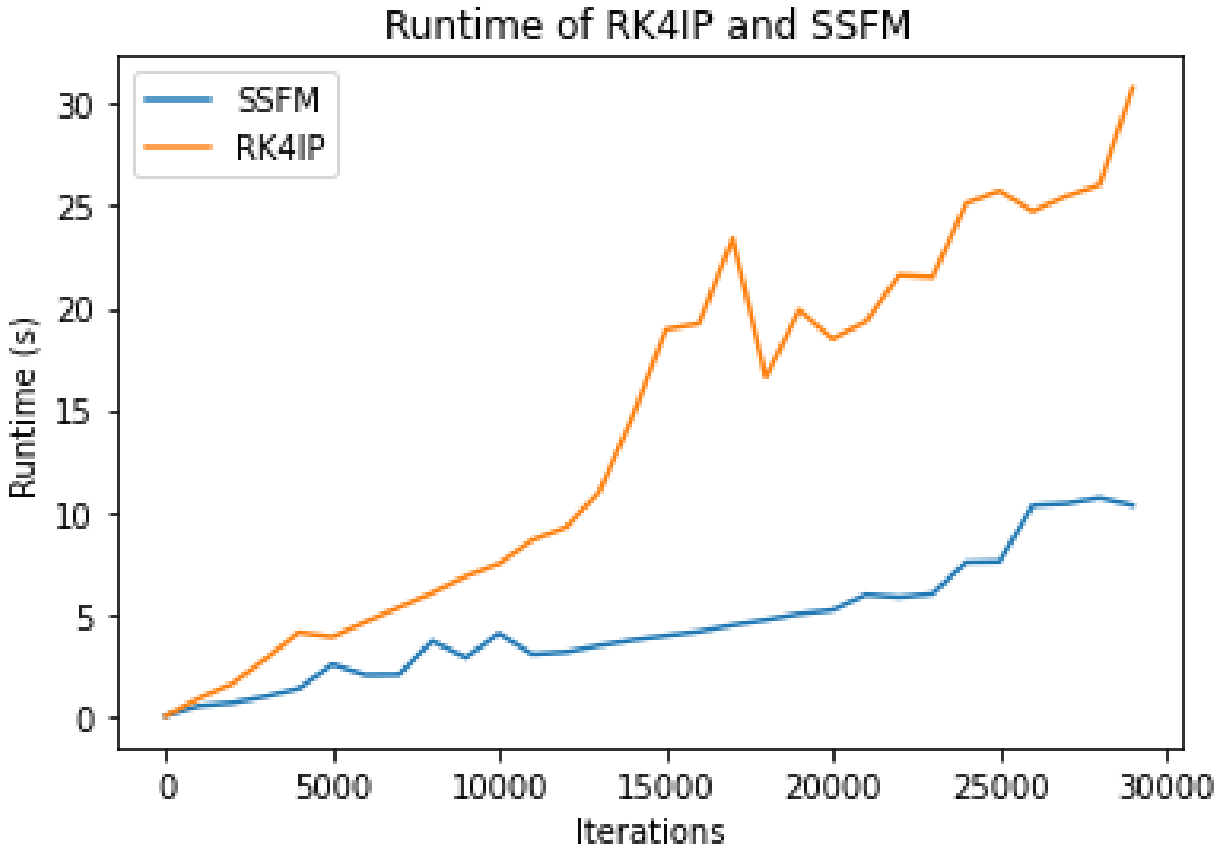

Figure 5.12: Runtime Comparison of SSFM Vs. RK4IP

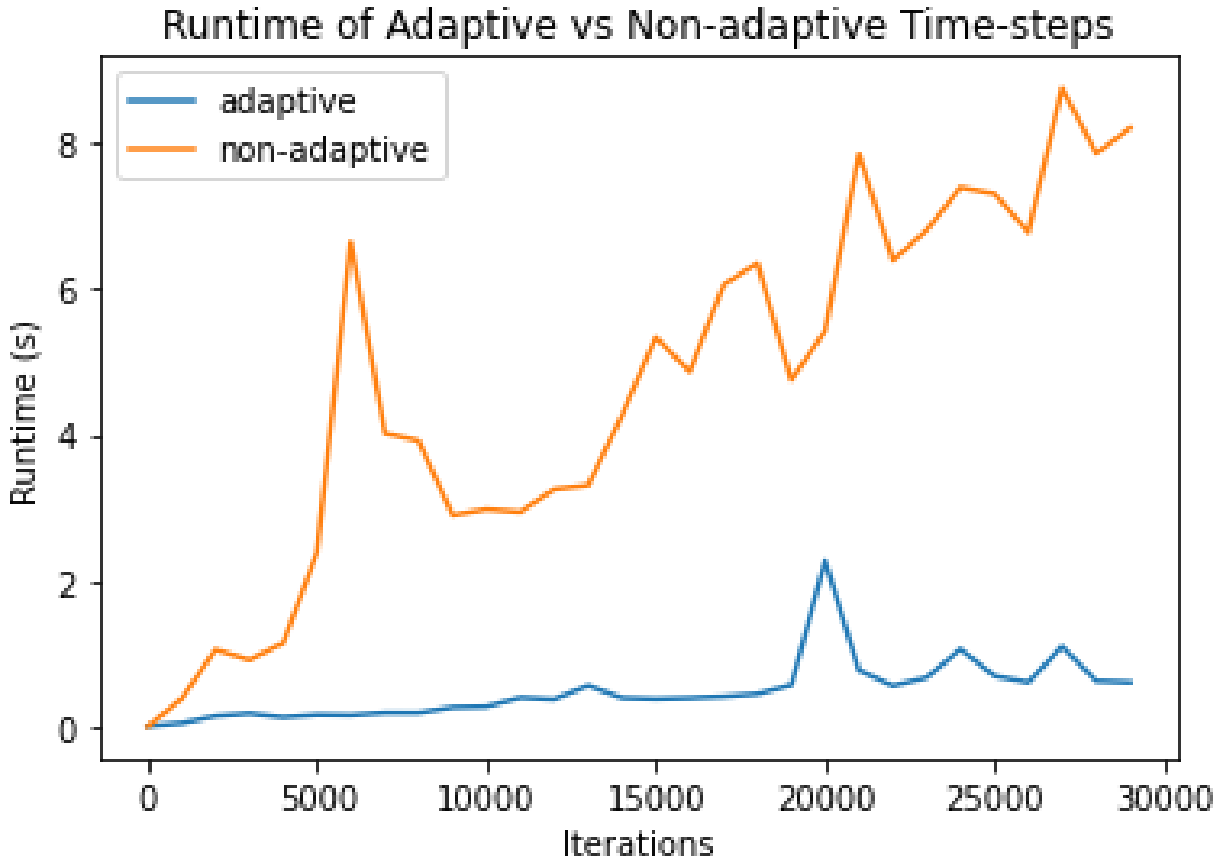

Figure 5.13: Runtime Comparison of Adaptive Vs. Non-Adaptive Time-Steps

6. Conclusion

6.1 Summary

This thesis provided a study of the dynamics of BECs as described by the GPE. The main delivery of this thesis is a software module in python that finds numerical solutions for the GPE. Along with this software module, this thesis aimed to simplify the exploration of BECs and to promote a greater understanding of their dynamics.

The background section of this thesis briefly presented a theoretical framework of BECs as well as the experimental techniques used to create them. And using the context of introductory quantum mechanics and the Pauli-exclusion principle, the GPE was introduced as a natural extension of the schrodinger equation in the context of BECs. This approach can also be extended to other non-linear forms of the schrodinger equation.

In the following section, this thesis discussed two approaches for numerically solving the GPE. The splitting step in the SSFM was presented as a solution that approximates the exponentiation of non-commuting operators, while the Fourier transformation was used to avoid expensive matrix exponentiation of the non-diagonal term in the kinetic operator of the Hamiltonian. On the other hand, the RK4IP was provided as result of a canonical transformation that simplified the GPE into a system of ordinary differential equations that can be solved with well-known time-stepping algorithms. This canonical transformation into the interaction picture was discussed as a unitary transformation and an extension of the Heisenberg picture. And the specific choice of using the RK4 method was made in order to reduce the number of Fourier transformations that would be included in the algorithm. Lastly, an adaptive time-step protocol is presented.

Section 4 introduced the imaginary time-step algorithm that is used to find the ground state solution of the BEC wave function. This algorithm uses the replacement of time with imaginary time in order to force higher energy states to decay faster than the ground state, thus converging to the ground state solution. The computational method for determining the level of the convergence of the imaginary time evolved wave function towards the ground state is also explained.

The last section provides several simulations that are made using the python application provided alongside this thesis. These simulations mainly visualize the process of finding the ground state solution and time evolution of the ground state caused by a change in the external potential. The result from these simulations mostly align with the expected

dynamics of BECs.

6.2 Outlook

The software package provided in this thesis allows for an easy exploration of the dynamics of BEC in a wide range of scenarios. The simulations shown in this thesis are not exhaustive of the countless ways in which the environment of a BEC can be structured. Therefore, it would be interesting to explore the dynamics of BECs in different combination of parameters and external potentials.

The major limitation facing numerical approaches comes from the iterative nature of a computational process. Although it is difficult to avoid this fact when dealing with numerical solutions, a variety of methods can be explored in order to reduce the runtime of the algorithms used in this thesis. These methods may include parallel processing or more efficient memory allocations so that the device executing these algorithms can efficiently use its resources. As such, it will be worthwhile to explore such techniques in order to make the SSFM and RK4IP algorithms more efficient.

A. Code Demonstration

A.1 1-D Implementation

```

from GPE_solver import *

# setting computational grid size and scattering length value
consts = Constants(dim=1, M=2**8, dx=5e-2, a_s=6e-3)
# initializing solution
sol = Solution(constants=consts, V=V_symmetric)
sol.vis.guessed_psi_plot()

# finding the ground state solution
sol.solve_ground_state(dt=(consts.dx**2)/10, lower_bound=1e-5)
sol.vis.guessed_vs_ground_psi_plot()

sol.ext_V = 0  # removing potential trap
# evolving the released BEC using RK4IP
sol.time_evolve(
    sol.ground_psi, 'RK4IP', dt=(consts.dx**2)/10, Nt=2000,
    snapshots=20, adaptive_step=False, dt_min=(consts.dx**2)/100)
# plotting 5 snapshots of the wave function density
sol.vis.psi_snapshots_plot_2d(plot_count=5)
# evolving the released BEC using SSFM
sol.time_evolve(
    sol.ground_psi, 'SSFM', dt=(consts.dx**2)/10, Nt=2000,
    snapshots=20, adaptive_step=False, dt_min=(consts.dx**2)/100)
# plotting 5 snapshots of the wave function density
sol.vis.psi_snapshots_plot_2d(plot_count=5)
```

A.2 2-D Implementation

```


from GPE_solver import *
import numpy as np

# setting computational grid size and scattering length value
```

```
consts = Constants(dim=2, M=2**4, dx=5e-1, a_s=6e-3)
# initializing solution
sol = Solution(constants=consts, V=V_symmetric)
sol.vis.guessed_psi_plot()

# finding the ground state solution
sol.solve_ground_state(dt=(consts.dx**2)/30, lower_bound=1e-5)
sol.vis.guessed_vs_ground_psi_plot()

sol.ext_V = 0  # removing potential trap
# evolving the released BEC using RK4IP
sol.time_evolve(
    sol.ground_psi, 'RK4IP', dt=(consts.dx**2)/30, Nt=200,snapshots=20,
    adaptive_step=False, dt_min=(consts.dx**2)/100)
# plotting 6 snapshots of the wave function density
sol.vis.heat_graph(6)
# evolving the released BEC using SSFM
sol.time_evolve(
    sol.ground_psi, 'SSFM', dt=(consts.dx**2)/30, Nt=200,snapshots=20,
    adaptive_step=False, dt_min=(consts.dx**2)/100)
# plotting 6 snapshots of the wave function density
sol.vis.heat_graph(6)

# shifting external potential
sol.ext_V = sol.generate_external_potential(V_shifted)
# evolving the released BEC using RK4IP
sol.time_evolve(
    sol.ground_psi,'RK4IP',dt=(consts.dx**2)/35,Nt=800,snapshots=20,
    adaptive_step=False, dt_min=(consts.dx**2)/100)
# plotting 6 snapshots of the wave function density
sol.vis.heat_graph(6)

# swiching isotropic potential with cigar shaped potential
sol.ext_V = sol.generate_external_potential(V_cigar_shaped)
# evolving the released BEC using RK4IP
sol.time_evolve(
    sol.ground_psi,'RK4IP',dt=(consts.dx**2)/35,Nt=1300,snapshots=20,
    adaptive_step=False, dt_min=(consts.dx**2)/100)
# plotting 6 snapshots of the wave function density
sol.vis.heat_graph(6)

sol.ext_V = 0  # removing potential trap
# evolving the released BEC with a shifted image of itself
sol.time_evolve_interference2(
    np.roll(sol.ground_psi,-7), np.roll(sol.ground_psi,7),
    'RK4IP',dt=(consts.dx**2)/35,Nt=250,snapshots=20,
    adaptive_step=False, dt_min=(consts.dx**2)/100)
# plotting 6 snapshots of the wave function density
sol.vis.heat_graph(6)
```

Bibliography

[1] C. C. Bradley, C. Sackett, J. Tollett, and R. G. Hulet, Physical review letters **75**, 1687 (1995).

[2] M. H. Anderson, J. R. Ensher, M. R. Matthews, C. E. Wieman, and E. A. Cornell, science **269**, 198 (1995).

[3] B. M. Caradoc-Davies, Ph.D. thesis, University of Otago (2000).

[4] A. Groszek, Ph.D. thesis, Monash University (2000).

[5] A. Griffin, D. W. Snoke, and S. Stringari, *Bose-einstein condensation* (Cambridge University Press, 1996).

[6] C. J. Pethick and H. Smith, *Bose–Einstein condensation in dilute gases* (Cambridge university press, 2008).

[7] I. G. Kaplan, *The Pauli exclusion principle: origin, verifications, and applications* (John Wiley & Sons, 2017).

[8] L. Susskind and A. Friedman, *Quantum mechanics: the theoretical minimum* (Basic Books, 2014).

[9] A. Altland and B. D. Simons, *Condensed matter field theory* (Cambridge university press, 2010).

[10] O. V. Sinkin, R. Holzlöhner, J. Zweck, and C. R. Menyuk, Journal of lightwave technology **21**, 61 (2003).

[11] M. Suzuki, Journal of Mathematical Physics **32**, 400 (1991).

[12] H. Stenlund, IOSR Journal of Mathematics (IOSR-JM) e-ISSN pp. 2278–5728 (2021).

[13] S. Balac, A. Fernandez, F. Mahé, F. Méhats, and R. Texier-Picard, ESAIM: Mathematical Modelling and Numerical Analysis **50**, 945 (2016).

[14] E. Zeidler, *Quantum field theory I: Basics in mathematics and physics: A bridge between mathematicians and physicists* (Springer, 2006).

[15] M. Tenenbaum and H. Pollard, *Ordinary differential equations: an elementary textbook for students of mathematics, engineering, and the sciences* (Courier Corporation, 1985).

[16] S. Balac and F. Mahé, Computer Physics Communications **184**, 1211 (2013).

[17] S. Balac and A. Fernandez, Optics Communications **329**, 1 (2014).